Observability Analysis of Collaborative Opportunistic Navigation With Pseudorange Measurements

Zaher M. Kassas, *Senior Member, IEEE*, and Todd E. Humphreys, *Member, IEEE*

***Abstract*—The observability analysis of a collaborative opportunistic navigation (COpNav) environment whose states may be partially known is considered. A COpNav environment can be thought of as a radio frequency (RF) signal landscape within which one or more RF receivers locate themselves in space and time by extracting and, possibly, sharing information from ambient signals of opportunity (SOPs). These receivers, whether vehicle mounted or integrated into handheld devices, exploit signal diversity to improve navigation and timing robustness compared with stand-alone Global Positioning System (GPS) receivers in deep urban, indoor, or, otherwise, GPS-hostile environments. Available SOPs may have a fully known, partially known, or unknown characterization. In this paper, the receivers are assumed to draw only pseudorange-type measurements from the SOPs. Separate observations are fused to produce an estimate of each receiver's position, velocity, and time (PVT). Since not all SOP states in the COpNav environment may be known *a priori*, the receivers must estimate the unknown SOP states of interest simultaneously with their own PVT. This paper establishes the minimal conditions under which a COpNav environment consisting of multiple receivers and multiple SOPs is completely observable. Moreover, in scenarios where the COpNav environment is unobservable, the unobservable directions in the state space are specified. Simulation and experimental results are presented to confirm the theoretical observability conditions.**

***Index Terms*—Collaborative opportunistic navigation (COpNav), estimation, Global Navigation Satellite Systems (GNSS), Global Positioning System (GPS), observability, radionavigation, signals of opportunity (SOP).**

I. Introduction

GLOBAL Navigation Satellite Systems (GNSSs) are insufficient for reliable anytime anywhere navigation, particularly in GNSS-challenged environments, such as indoors, deep urban canyons, and GNSS-denied environments experiencing intentional jamming. Several approaches have been proposed to address the inherent limitations of GNSS-based navigation, most notably augmenting GNSS receivers with dead-reckoning systems and map-matching algorithms [1]–[5]. Motivated by the plenitude of ambient RF signals, a new paradigm to overcome the limitations of GNSS-based navigation, which is termed opportunistic navigation (OpNav), has been proposed [6]. This paradigm aims to extract positioning and timing information from ambient RF "signals of opportunity" (SOPs) to improve navigation and timing robustness compared with stand-alone GNSS receivers. OpNav radio receivers, which may be vehicle mounted or hand carried, continuously search for opportune signals from which to draw navigation and timing information, employing on-the-fly signal characterization as necessary. Signals from discovered SOPs are downmixed and sampled coherently, yielding a tight coupling between signal streams that permits carrier-phase-level fusion of observables from the various streams within a single or distributed state estimator. In collaborative OpNav (COpNav), multiple OpNav receivers share information to construct and continuously refine a global signal landscape [7]. In this paper, localization and timing are treated in absolute world-centric spatial and temporal frames. This is motivated by the fact that the ultimate objective of COpNav is to build a global signal landscape map, which any receiver can tap into and contribute to.

In its most general form, OpNav treats all ambient radio signals as potential SOPs, from conventional GNSS signals to communication signals that are never intended for use as timing or positioning sources, such as iridium satellite signals [8], digital television signals [9], and cellular signals [10]. The relative timing and frequency offsets, transmit location, and frequency stability of each signal are estimated on the fly as necessary, with prior information about these quantities exploited when available. At this level of generality, the OpNav estimation problem is similar to the so-called simultaneous localization and mapping (SLAM) problem in robotics [11], [12]. Both imagine an agent that, starting with incomplete knowledge of its location and surroundings, builds a map of its environment and simultaneously locates itself within that map.

In traditional SLAM, the map that is constructed as the agent (typically a robot) moves through the environment is composed of landmarks, such as walls, corners, and posts, with associated positions. OpNav extends this concept to radio signals, with

Manuscript received February 11, 2013; revised June 13, 2013; accepted August 2, 2013. Date of publication September 20, 2013; date of current version January 31, 2014. This work was supported in part by the Wireless Networking and Communication Group (WNCG) through the WNCG Industrial Affiliates Program and in part by the National Science Foundation through the Industry and University Cooperative Research Program Wireless Internet Center for Advanced Technology under Grant IIP-1067914. The Associate Editor for this paper was X. Zhang.

Z. M. Kassas is with the Department of Electrical and Computer Engineering and also with the University of Texas Radionavigation Laboratory, The University of Texas at Austin, Austin, TX 78712 USA (e-mail: zkassas@ieee.org).

T. E. Humphreys is with the Department of Aerospace Engineering and Engineering Mechanics and also with the University of Texas Radionavigation Laboratory, The University of Texas at Austin, Austin, TX 78712 USA (e-mail: todd.humphreys@mail.utexas.edu).

Color versions of one or more of the figures in this paper are available online at http://ieeexplore.ieee.org.

Digital Object Identifier 10.1109/TITS.2013.2278293

SOPs playing the role of landmarks. In contrast to a SLAM environmental map, which can be extracted from a cluttered dynamic environment but, ultimately, must be composed of fixed landmarks [13], [14], the OpNav "signal landscape" is dynamic and more complex. For the simple case of pseudorange-only OpNav, where observables consist solely of signal time-of-arrival measurements, one must estimate, in addition to the three-dimensional (3-D) position $\boldsymbol{r}_s$ and velocity $\dot{\boldsymbol{r}}_s$ of each SOP transmitter's antenna, each SOP's time offset δt_s from a reference time base, the rate of change of time offset $\dot{\delta t}_s$, and a small set of parameters that characterize the SOP's reference oscillator stability. In addition, more SOP parameters are required for an OpNav framework in which both pseudorange and carrier phase measurements are ingested into the estimator [6]. Of course, in addition to the SOP parameters, the OpNav receiver's own 3-D position $\boldsymbol{r}_r$ and velocity $\dot{\boldsymbol{r}}_r$, time offset δt_r, and time offset rate $\dot{\delta t}_r$ must be estimated.

The GPS control segment routinely solves an instance of the OpNav problem: the location and timing offsets of a dozen or more GPS ground stations are simultaneously estimated, together with the orbital and clock parameters of the GPS satellites [15]. Compared with the general OpNav problem, the GPS control segment's problem enjoys the constraints imposed by accurate prior estimates of site locations and satellite orbits. Moreover, estimation of clock states is aided by the presence of highly stable atomic clocks in the satellites and at each ground station. In contrast, an OpNav receiver entering a new signal landscape may have less prior information to exploit and, typically, cannot assume atomic frequency references, either for itself or for the SOPs. The GPS control segment example also highlights the essentially collaborative nature of COpNav. Similar to the GPS ground stations, multiple COpNav receivers can share information to construct and continuously refine a global signal landscape.

The large size of the COpNav estimation problem, which may involve hundreds of states, naturally raises the question of state observability. A study of COpNav observability benefits from the COpNav–SLAM analogy. Although the question of observability was not addressed for more than a decade after SLAM was introduced, the recent SLAM literature has come around to considering fundamental properties of the SLAM problem, including observability [16]–[24]. The effects of partial observability in planar SLAM with range and bearing measurements were first analyzed via linearization in [16] and [17]. These papers came to the counterintuitive conclusion that the two-dimensional (2-D) planar world-centric (absolute reference frame) SLAM problem is fully observable when the location of a single landmark is known *a priori*. With a nonlinear observability analysis, this result was subsequently disproved, and it was shown that at least two anchor landmarks with known positions are required for local weak observability [19]. Later analysis of the SLAM problem's Fisher information matrix (FIM) confirmed the result of the nonlinear analysis [20]. However, an apparent discrepancy between linear and nonlinear SLAM observability reemerged in [21], where it was shown that a linear analysis based on piecewise constant system (PWCS) theory [25] again predicted global planar SLAM observability in the case of a single known anchor landmark, whereas a nonlinear analysis in the same paper indicated that two known anchor landmarks were required for local weak observability. However, no explanation for the reasons behind such discrepancies was offered. The linear PWCS result appears flawed since an observability test based on linearization should never predict observability in a case where a nonlinear test indicates lack of observability.

An initial OpNav observability analysis was conducted in [26]. It considered an OpNav environment comprising a single receiver and multiple stationary SOPs. This OpNav observability analysis utilized nonlinear local weak observability tests, linear time-varying (LTV) observability tests, and PWCS observability tests. While the conclusions achieved by the former two methods agreed, the PWCS observability tests yielded contradictory results, similar to those encountered in the SLAM literature. The paper concluded that PWCS observability theory is inapplicable to systems whose measurement model is nonlinear. Thus, it is improperly applied in [18], and this explains the contradictory observability results in [21]. The observability analysis was later extended to the case of multiple receivers in a COpNav environment, and the degree of observability, which is also known as estimability, of the various states in the environment was quantified, with special attention paid to the least and most observable states [27]. However, the observability results in [27] were offered without any rigorous proofs, and only single-run extended Kalman filter (EKF) sample path simulations were presented.

This paper extends the work of [27] in three different ways. First, it analyzes the observability of various scenarios that could be encountered in a typical COpNav environment comprising multiple receivers and multiple SOPs. For each scenario, the following questions are answered and proven rigorously: 1) Is the environment observable; and 2) if the environment is not completely observable, what are the unobservable directions in the state space? Second, single-run and Monte Carlo (MC)-based simulations are presented, which agree with the theoretical observability analysis. Third, experimental results are presented, which also agree with the theoretical observability analysis. The experimental results illustrate an important outcome of this paper's analysis, i.e., a receiver with known initial state that is moving according to velocity random-walk dynamics and making pseudorange observations on unknown SOPs in the environment can estimate the states of such SOPs.

The remainder of this paper is organized as follows. Section II gives an overview of the various notions and tools that are of relevance in analyzing the observability of COpNav environments: nonlinear observability, LTV observability, PWCS observability, stochastic observability, and estimability. Section III describes the COpNav environment dynamics and observation models considered in this paper. Section IV analyzes various COpNav scenarios and establishes whether each scenario is observable. This leads to a set of minimum conditions necessary for complete COpNav observability. Section V presents simulation results on a number of scenarios. Section VI presents experimental results illustrating an important outcome of this paper's observability conclusions. Concluding remarks are given in Section VII.

II. Theoretical Background: Observability Measures

Here, an overview of various observability measures of dynamic systems and their associated tests is given, which are of relevance in analyzing the observability of COpNav environments.

Conceptually, observability of a dynamic system boils down to the question of solvability of the state from a set of observations that are linearly or nonlinearly related to the state, and where the state evolves according to a set of linear or nonlinear difference or differential equations. In particular, observability is concerned with determining whether the state of the system can be consistently estimated from a set of observations taken over a finite period of time.

A. Observability of Nonlinear Systems

Various notions of observability exist for continuous-time (CT) nonlinear dynamic systems. Consider the system

$$\Sigma_{\mathrm{NL}}: \begin{cases} \dot{\boldsymbol{x}}(t) = \boldsymbol{f}\left[\boldsymbol{x}(t), \boldsymbol{u}(t)\right], & \boldsymbol{x}(t_0) = \boldsymbol{x}_0 \\ \boldsymbol{y}(t) = \boldsymbol{h}\left[\boldsymbol{x}(t)\right], \end{cases} \tag{1}$$

where $\boldsymbol{x} \in \mathbb{R}^n$ is the system state vector, $\boldsymbol{u} \in \mathbb{R}^r$ is the control input vector, $\boldsymbol{y} \in \mathbb{R}^m$ is the observation vector, and $\boldsymbol{x}_0$ is an arbitrary initial condition. This system may be characterized as observable, locally observable, weakly observable, or locally weakly observable [28]. A somewhat simple algebraic test based on Lie derivatives exists for establishing local weak observability of a specific form of the nonlinear system Σ_{NL} in (1), which is known as the control affine form, in which the control inputs affect the dynamics additively [29]. This test was applied to analyze the observability of SLAM environments in [19] and [21] and of OpNav environments in [26]. It is worth noting that local observability is a sufficient condition (but not necessary) to establish local weak observability.

B. Observability of Linear Systems

Observability of discrete-time (DT) LTV systems is defined as follows [30].

Definition II.1: Consider the DT LTV dynamic system

$$\Sigma_L: \begin{cases} \boldsymbol{x}(t_{k+1}) = \mathbf{F}(t_k)\boldsymbol{x}(t_k) + \mathbf{G}(t_k)\boldsymbol{u}(t_k), & \boldsymbol{x}(t_{k_0}) = \boldsymbol{x}_0 \\ \boldsymbol{y}(t_k) \quad\;\; = \mathbf{H}(t_k)\boldsymbol{x}(t_k), & t_k \in [t_{k_0}, t_{k_f}] \end{cases} \tag{2}$$

where $\mathbf{F} \in \mathbb{R}^{n\times n}$, $\mathbf{G} \in \mathbb{R}^{n\times r}$, and $\mathbf{H} \in \mathbb{R}^{m\times n}$. LTV system Σ_L is said to be observable in the time interval $[t_{k_0}, t_{k_f}]$ if the initial state $\boldsymbol{x}_0$ is uniquely determined by the zero-input response $\boldsymbol{y}(t_k)$ for $t_k \in [t_{k_0}, t_{k_f-1}]$. If this property holds regardless of the initial time t_{k_0} or the initial state $\boldsymbol{x}_0$, the system is said to be completely observable.

Observability of LTV systems Σ_L is typically established through studying the rank of either the so-called observability Grammian or the observability matrix. The following theorem states a necessary and sufficient condition for observability of LTV systems through the l-step observability matrix [30].

Theorem II.1: The LTV system Σ_L is l-step observable if and only if the l-step observability matrix, which is defined as

$$\boldsymbol{\mathcal{O}}_L(t_k, t_{k+l}) \triangleq \begin{bmatrix} \mathbf{H}(t_k) \\ \mathbf{H}(t_{k+1})\boldsymbol{\Phi}(t_{k+1}, t_k) \\ \vdots \\ \mathbf{H}(t_{k+l-1})\boldsymbol{\Phi}(t_{k+l-1}, t_k) \end{bmatrix} \tag{3}$$

is full rank, i.e., $\mathrm{rank}[\boldsymbol{\mathcal{O}}_L(t_k, t_{k+l})] = n$. The matrix function $\boldsymbol{\Phi}$ is the DT transition matrix, which is defined as

$$\boldsymbol{\Phi}(t_k, t_j) \triangleq \begin{cases} \mathbf{F}(t_{k-1})\mathbf{F}(t_{k-2})\cdots\mathbf{F}(t_j), & t_k \geq t_{j+1} \\ \mathbf{I}, & t_k = t_j. \end{cases}$$

Linear observability tools may be applied to nonlinear systems by expressing the nonlinear system in its linearized error (perturbation) form. In this formulation, the state vector $\Delta\boldsymbol{x}$, the control input vector $\Delta\boldsymbol{u}$, and the observation vector $\Delta\boldsymbol{y}$ are defined as the difference between the true and nominal states, between the true and nominal inputs, and between the true and nominal observations, respectively. The discretized version of the linearized error form of Σ_{NL} in (1) is given by

$$\begin{aligned} \Delta\boldsymbol{x}(t_{k+1}) &= \mathbf{F}(t_k)\,\Delta\boldsymbol{x}(t_k) + \mathbf{G}(t_k)\,\Delta\boldsymbol{u}(t_k) \\ \Delta\boldsymbol{y}(t_k) &= \mathbf{H}(t_k)\Delta\boldsymbol{x}(t_k), \end{aligned} \tag{4}$$

where $\mathbf{F}$, $\mathbf{G}$, and $\mathbf{H}$ are the dynamics, input, and observation Jacobian matrices, respectively, evaluated at the nominal states and inputs. The observability results achieved in this case are only valid locally.

It was demonstrated in [27] that the l-step observability test applied to an error-form COpNav environment yields identical results to those achieved by the more complicated Lie-derivative-based nonlinear local weak observability test. Therefore, in this paper's analysis, observability will be established via the l-step method. The remaining three observability notions introduced here are presented either because they have been misapplied in previous COpNav-like observability analyses (PWCS observability) or because they complete the set of observability notions that could profitably be applied to the present analysis (stochastic observability and estimability).

C. Observability of Linear Piecewise Constant Systems

If the matrices $\mathbf{F}$, $\mathbf{G}$, and $\mathbf{H}$ in (2) are piecewise constant over every time segment j, i.e., if $\mathbf{F}(t_k) = \mathbf{F}_j$, $\mathbf{G}(t_k) = \mathbf{G}_j$, and $\mathbf{H}(t_k) = \mathbf{H}_j$ for $t_k \in [t_{k_j}, t_{k_j+n-1}]$, but may vary from one segment to another, then the LTV system Σ_L is said to be a PWCS. In [25], simple necessary and sufficient conditions to establish observability of CT and DT PWCSs were derived, which are based on the so-called total observability matrix and the stripped observability matrix. While the PWCS observability tests are attractive due to their simplicity, they have been improperly applied to nonlinear dynamic systems in the SLAM literature, leading to the contradictory results in [16]–[21]. As clarified in [26], the reason behind the discrepancies is that one cannot simply take time segment j to coincide with a single discretization instant t_k. Rather, each time segment j must contain at least n measurement samples during the collection

of which the Jacobian matrices $\mathbf{F}$, $\mathbf{G}$, and $\mathbf{H}$ can be accurately modeled as constant.

D. Stochastic Observability via Fisher Information

From an estimation theoretic point of view, the FIM quantifies the maximum existing information in observations about the system's random state. A singular FIM implies that the Cramér–Rao lower bound does not exist as the FIM's inverse has one or more infinite eigenvalues, which means total uncertainty in a subspace of the state space. This amounts to the information being insufficient for the estimation problem under consideration [31]. In [20], the nonlinear SLAM problem was recast as a problem of estimating a set of unknown, constant random variables for which the FIM was derived and analyzed to assess observability. Under Gaussian assumptions and minimum-mean-square-error estimation, the FIM is the inverse of the estimation error covariance matrix. Hence, another assessment of observability can be achieved by analyzing the information form of the Kalman filter (KF). If the system is observable, then the information matrix will eventually become invertible. This approach to analyzing observability was adopted for SLAM observability analysis in [22] and [23].

E. Degree of Observability: Estimability

Whereas the notion of observability is a Boolean property, i.e., it specifies whether the system is observable or not, for estimation purposes, the question of estimability is of considerable importance. Estimability assesses the "degree of observability" of the various states. Estimability can be assessed by the condition number of the FIM, thus measuring whether an observable system is poorly estimable due to the gradient vectors comprising the FIM being nearly collinear [31]. Alternatively, estimability can be assessed by analyzing the eigenvalues and eigenvectors of the estimation error covariance matrix of the KF estimating the states of the system of interest. In particular, the largest eigenvalue corresponds to the variance of the state or the linear combination of states with the poorest observability. On the other hand, the state or the linear combination of states with the most observability is indicated by the smallest eigenvalue. The appropriate linear combination of states yielding the calculated degree of observability is given by the respective eigenvectors [32]. The estimability of COpNav environments was studied in [27].

III. Model Description

A. Dynamics Model

The receiver's dynamics will be assumed to evolve according to the velocity random-walk model. An object moving according to such dynamics in generic coordinate ξ has the dynamics

$$\ddot{\xi}(t) = \tilde{w}_\xi(t)$$

where $\tilde{w}_\xi(t)$ is a zero-mean white noise process with power spectral density $\tilde{q}_\xi$, i.e.,

$$\mathbb{E}\left[\tilde{w}_\xi(t)\right] = 0, \qquad \mathbb{E}\left[\tilde{w}_\xi(t)\tilde{w}_\xi(\tau)\right] = \tilde{q}_\xi\,\delta(t-\tau)$$

where $\delta(t)$ is the Dirac delta function. The receiver and SOP clock error dynamics will be modeled according to the so-called two-state model, which is composed of clock bias δt and clock drift $\dot{\delta t}$. The clock error states evolve according to

$$\dot{\boldsymbol{x}}_{\text{clk}}(t) = \mathbf{A}_{\text{clk}}\,\boldsymbol{x}_{\text{clk}}(t) + \tilde{\boldsymbol{w}}_{\text{clk}}(t)$$

where

$$\boldsymbol{x}_{\text{clk}} = \begin{bmatrix} \delta t \\ \dot{\delta t} \end{bmatrix} \quad \tilde{\boldsymbol{w}}_{\text{clk}} = \begin{bmatrix} \tilde{w}_{\delta t} \\ \tilde{w}_{\dot{\delta t}} \end{bmatrix} \quad \mathbf{A}_{\text{clk}} = \begin{bmatrix} 0 & 1 \\ 0 & 0 \end{bmatrix}$$

where $\tilde{w}_{\delta t}$ and $\tilde{w}_{\dot{\delta t}}$ are modeled as zero-mean mutually independent white noise processes with power spectra $S_{\tilde{w}_{\delta t}}$ and $S_{\tilde{w}_{\dot{\delta t}}}$, respectively. The power spectra $S_{\tilde{w}_{\delta t}}$ and $S_{\tilde{w}_{\dot{\delta t}}}$ can be related to the power-law coefficients $\{h_\alpha\}_{\alpha=-2}^{2}$, which have been shown through laboratory experiments to characterize the power spectral density of the fractional frequency deviation $y(t)$ of an oscillator from nominal frequency, namely, $S_y(f) = \sum_{\alpha=-2}^{2} h_\alpha f^\alpha$ [33], [34]. It is common to approximate such relationships by considering only the frequency random-walk coefficient h_{-2} and the white frequency coefficient h_0, which lead to $S_{\tilde{w}_{\delta t}} \approx h_0/2$ and $S_{\tilde{w}_{\dot{\delta t}}} \approx 2\pi^2 h_{-2}$ [31], [35].

The receiver's state vector will be defined by augmenting the receiver's planar position and velocity states with its clock error states to yield the state space realization

$$\dot{\boldsymbol{x}}_r(t) = \mathbf{A}_r\,\boldsymbol{x}_r(t) + \mathbf{D}_r\,\tilde{\boldsymbol{w}}_r(t) \tag{5}$$

where $\boldsymbol{x}_r = [\boldsymbol{r}_r^\mathsf{T},\ \dot{\boldsymbol{r}}_r^\mathsf{T},\ \delta t_r,\ \dot{\delta t}_r]^\mathsf{T}$, $\boldsymbol{r}_r = [x_r,\ y_r]^\mathsf{T}$, $\tilde{\boldsymbol{w}}_r = [\tilde{w}_x,\ \tilde{w}_y,\ \tilde{w}_{\delta t_r},\ \tilde{w}_{\dot{\delta t}_r}]^\mathsf{T}$

$$\mathbf{A}_r = \begin{bmatrix} \mathbf{0}_{2\times2} & \mathbf{I}_{2\times2} & \mathbf{0}_{2\times2} \\ \mathbf{0}_{2\times2} & \mathbf{0}_{2\times2} & \mathbf{0}_{2\times2} \\ \mathbf{0}_{2\times2} & \mathbf{0}_{2\times2} & \mathbf{A}_{\text{clk}} \end{bmatrix} \quad \mathbf{D}_r = \begin{bmatrix} \mathbf{0}_{2\times4} \\ \mathbf{I}_{4\times4} \end{bmatrix}.$$

The receiver's dynamics in (5) is discretized at a constant sampling period $T \triangleq t_{k+1} - t_k$ to yield the DT model

$$\boldsymbol{x}_r(t_{k+1}) = \mathbf{F}_r\,\boldsymbol{x}_r(t_k) + \boldsymbol{w}_r(t_k), \quad k = 0, 1, 2, \ldots \tag{6}$$

where $\boldsymbol{w}_r$ is a DT zero-mean white noise sequence with covariance $\mathbf{Q}_r = \text{diag}[\mathbf{Q}_{\text{pv}},\ \mathbf{Q}_{\text{clk},r}]$, with

$$\mathbf{F}_r = \begin{bmatrix} \mathbf{I}_{2\times2} & T\mathbf{I}_{2\times2} & \mathbf{0}_{2\times2} \\ \mathbf{0}_{2\times2} & \mathbf{I}_{2\times2} & \mathbf{0}_{2\times2} \\ \mathbf{0}_{2\times2} & \mathbf{0}_{2\times2} & \mathbf{F}_{\text{clk}} \end{bmatrix} \quad \mathbf{F}_{\text{clk}} = \begin{bmatrix} 1 & T \\ 0 & 1 \end{bmatrix}$$

$$\mathbf{Q}_{\text{clk},r} = \begin{bmatrix} S_{\tilde{w}_{\delta t_r}} T + S_{\tilde{w}_{\dot{\delta t}_r}} \frac{T^3}{3} & S_{\tilde{w}_{\dot{\delta t}_r}} \frac{T^2}{2} \\ S_{\tilde{w}_{\dot{\delta t}_r}} \frac{T^2}{2} & S_{\tilde{w}_{\dot{\delta t}_r}} T \end{bmatrix}$$

$$\mathbf{Q}_{\text{pv}} = \begin{bmatrix} \tilde{q}_x \frac{T^3}{3} & 0 & \tilde{q}_x \frac{T^2}{2} & 0 \\ 0 & \tilde{q}_y \frac{T^3}{3} & 0 & \tilde{q}_y \frac{T^2}{2} \\ \tilde{q}_x \frac{T^2}{2} & 0 & \tilde{q}_x T & 0 \\ 0 & \tilde{q}_y \frac{T^2}{2} & 0 & \tilde{q}_y T \end{bmatrix}.$$

The SOP will be assumed to emanate from a spatially stationary terrestrial transmitter, and its state will consist of its planar position and clock error states. Hence, the SOP's dynamics can be described by the state space model

$$\dot{\boldsymbol{x}}_s(t) = \mathbf{A}_s\,\boldsymbol{x}_s(t) + \mathbf{D}_s\tilde{\boldsymbol{w}}_s(t) \tag{7}$$

where $\boldsymbol{x}_s = [\boldsymbol{r}_s^{\mathsf{T}},\ \delta t_s,\ \dot{\delta} t_s]^{\mathsf{T}}$, $\boldsymbol{r}_s = [x_s,\ y_s]^{\mathsf{T}}$, $\boldsymbol{w}_s = [\tilde{w}_{\delta t_s},\ \tilde{w}_{\dot{\delta} t_s}]^{\mathsf{T}}$

$$\mathbf{A}_s = \begin{bmatrix} \mathbf{0}_{2\times 2} & \mathbf{0}_{2\times 2} \\ \mathbf{0}_{2\times 2} & \mathbf{A}_{\text{clk}} \end{bmatrix} \quad \mathbf{D}_s = \begin{bmatrix} \mathbf{0}_{2\times 2} \\ \mathbf{I}_{2\times 2} \end{bmatrix}.$$

Discretizing the SOP's dynamics (7) at a sampling interval T yields the DT-equivalent model

$$\boldsymbol{x}_s(t_{k+1}) = \mathbf{F}_s\, \boldsymbol{x}_s(t_k) + \boldsymbol{w}_s(t_k) \tag{8}$$

where $\boldsymbol{w}_s$ is a DT zero-mean white noise sequence with covariance $\mathbf{Q}_s$, and

$$\mathbf{F}_s = \text{diag}[\mathbf{I}_{2\times 2},\ \mathbf{F}_{\text{clk}}] \quad \mathbf{Q}_s = \text{diag}[\mathbf{0}_{2\times 2},\ \mathbf{Q}_{\text{clk,s}}]$$

where $\mathbf{Q}_{\text{clk},s}$ is identical to $\mathbf{Q}_{\text{clk},r}$, except that $S_{\tilde{w}_{\delta t_r}}$ and $S_{\tilde{w}_{\dot{\delta} t_r}}$ are now replaced with SOP-specific spectra $S_{\tilde{w}_{\delta t_s}}$ and $S_{\tilde{w}_{\dot{\delta} t_s}}$, respectively.

Defining the augmented state as $\boldsymbol{x} \triangleq [\boldsymbol{x}_r^{\mathsf{T}},\ \boldsymbol{x}_s^{\mathsf{T}}]^{\mathsf{T}}$ and the augmented process noise vector as $\boldsymbol{w} \triangleq [\boldsymbol{w}_r^{\mathsf{T}},\ \boldsymbol{w}_s^{\mathsf{T}}]^{\mathsf{T}}$ yields the system dynamics

$$\boldsymbol{x}(t_{k+1}) = \mathbf{F}\, \boldsymbol{x}(t_k) + \boldsymbol{w}(t_k) \tag{9}$$

where $\mathbf{F} = \text{diag}[\mathbf{F}_r,\ \mathbf{F}_s]$, and $\boldsymbol{w}$ is a zero-mean white noise sequence with covariance $\mathbf{Q} = \text{diag}[\mathbf{Q}_r,\ \mathbf{Q}_s]$. While the model defined in (9) considered only one receiver and one SOP, the model can be readily extended to multiple receivers and multiple SOPs by augmenting their corresponding states.

B. Observation Model

To properly model the pseudorange observations, one must consider three different time systems. The first is true time, which is denoted t and can be considered equivalent to the GPS system time. The second time system is that of the receiver's clock and is denoted t_r. The third time system is that of the SOP's clock and is denoted t_s. The three time systems are related to each other according to

$$t = t_r - \delta t_r(t) \qquad t = t_s - \delta t_s(t) \tag{10}$$

where $\delta t_r(t)$ and $\delta t_s(t)$ are the amount by which the receiver and SOP clocks are different from true time, respectively.

The pseudorange observation made by the receiver on a particular SOP is made in the receiver time and is modeled according to

$$\begin{aligned}\rho(t_r) = &\left\|\boldsymbol{r}_r\left[t_r - \delta t_r(t_r)\right] - \boldsymbol{r}_s\left[t_r - \delta t_r(t_r) - \delta t_{\text{TOF}}\right]\right\|_2 \\ &+ c\left\{\delta t_r(t_r) - \delta t_s\left[t_r - \delta t_r(t_r) - \delta t_{\text{TOF}}\right]\right\} + \tilde{v}_\rho(t_r)\end{aligned} \tag{11}$$

where c is the speed of light, δt_{TOF} is the time of flight of the signal from the SOP to the receiver, and $\tilde{v}_\rho$ is the error in the pseudorange measurement due to modeling and measurement errors. The error $\tilde{v}_\rho$ is modeled as a zero-mean white Gaussian noise process with power spectral density $\tilde{r}$ [36]. In (11), the clock offsets δt_r and δt_s were assumed to be small and slowly changing, in which case $\delta t_r(t) = \delta t_r[t_r - \delta t_r(t)] \approx \delta t_r(t_r)$. The first term in (11) is the true range between the receiver's position at the time of reception and the SOP's position at the time of transmission of the signal, whereas the second term arises due to the offsets from true time in the receiver and SOP clocks.

The observation model in the form of (11) is inappropriate for our observability analysis as it suffers from two shortcomings: 1) It is in a time system that is different from the one considered in deriving the system dynamics; and 2) the observation model is a nonlinear function of the delayed system states. The first shortcoming can be dealt with by converting the observation model to true time. The second problem is commonly referred to as the output delay problem, in which the observations (outputs) are a delayed version, deterministic or otherwise, of the system state. A common approach to deal with this problem entails discretization and state augmentation [37]. For simplicity and in order not to introduce additional states in our model, proper approximations will be invoked to deal with the second shortcoming.

To this end, the pseudorange observation model in (11) is converted to true time by invoking the relationship (10) to get an observation model for $\rho[t + \delta t_r(t)]$. The resulting observation model is delayed by $\delta t_r(t)$ to get an observation model for $\rho(t)$. Assuming the receiver's position to be approximately stationary within a time interval of $\delta t_r(t)$, i.e., $\boldsymbol{r}_r[t - \delta t_r(t)] \approx \boldsymbol{r}_r(t)$ and using the fact that the SOP's position is stationary, i.e., $\boldsymbol{r}_s[t - \delta t_r(t) - \delta t_{\text{TOF}}] = \boldsymbol{r}_s(t)$, yields

$$\begin{aligned}\rho(t) \approx &\left\|\boldsymbol{r}_r(t) - \boldsymbol{r}_s(t)\right\|_2 \\ &+ c\left\{\delta t_r(t) - \delta t_s\left[t - \delta t_r(t) - \delta t_{\text{TOF}}\right]\right\} + \tilde{v}_\rho(t).\end{aligned} \tag{12}$$

Next, it is argued that $\delta t_s[t - \delta t_r(t) - \delta t_{\text{TOF}}] \approx \delta t_s(t)$. The validity of this argument depends on the size of δt_r and of δt_{TOF} and on the rate of change of δt_s. For ground-based SOP transmitters up to 1 km away, the time-of-flight δt_{TOF} is less than 3.34 μs. Likewise, the offset δt_r can be assumed to be on the order of microseconds. It is reasonable to assume SOP clock bias δt_s to have an approximately constant value over microsecond time intervals. Therefore, the pseudorange observation model can be further simplified and expressed as a nonlinear function of the state as

$$\begin{aligned}z(t) = \rho(t) &\triangleq h\left[\boldsymbol{x}(t)\right] + \tilde{v}_\rho(t) \\ &\approx \left\|\boldsymbol{r}_r(t) - \boldsymbol{r}_s(t)\right\|_2 + c\cdot\left[\delta t_r(t) - \delta t_s(t)\right] + \tilde{v}_\rho(t).\end{aligned} \tag{13}$$

Discretizing the observation equation (13) at a constant sampling interval T yields the DT-equivalent observation model

$$\begin{aligned}z(t_k) &= y(t_k) + v_\rho(t_k) \\ &= \left\|\boldsymbol{r}_r(t_k) - \boldsymbol{r}_s(t_k)\right\|_2 + c\cdot\left[\delta t_r(t_k) - \delta t_s(t_k)\right] + v_\rho(t_k)\end{aligned} \tag{14}$$

where v_ρ is a DT zero-mean white Gaussian process with covariance $r = \tilde{r}/T$.

It is worth noting that the main sources of error affecting pseudorange observations include uncertainties associated with the propagation medium (path delay and loss), receiver noise, multipath propagation, nonline-of-sight (NLOS) propagation,

multiple-access interference, and near-far effects. The effects of such error sources and mitigation methods are beyond the scope of this paper, but relevant discussions can be found in [10], [38]–[41], and the references therein.

IV. Observability Analysis of COpNav Environments

A. Observability Analysis Objective

Here, the various conditions under which a COpNav environment is observable are established. The objective of this analysis is twofold: 1) Determine whether the environment is observable; and 2) if the environment is not completely observable, determine the unobservable directions in the state space. To this end, the l-step observability matrix defined in Theorem II.1, which only considers the deterministic part of the system, will be utilized. It is worth noting that the results achieved in the upcoming analysis are valid only locally, i.e., within a neighborhood around the system's initial state. In particular, concluding that the system is observable should be interpreted in the context of the existence of a neighborhood within which the initial states are distinguishable. The contours of this neighborhood depend on the layout of the COpNav environment. For example, a planar environment with two SOP transmitters divides into two neighborhoods, one on either side of the line connecting the two transmitters [26].

B. Receiver Trajectory Singularity

In the upcoming analysis, it is assumed that the receiver is not stationary and that its trajectory is not collinear with the vectors connecting the receiver and any of the SOPs. It is assumed that $\nexists\ \alpha \in \mathbb{R}$ such that $\dot{x}_r(t_{k+1}) = \alpha[x_r(t_k) - x_s(t_k)]$ and $\dot{y}_r(t_{k+1}) = \alpha[y_r(t_k) - y_s(t_k)]$. This ensures that the bearing angle between the receiver and the SOPs is never constant along the receiver trajectory. This assumption ensures that the observability matrix will not lose rank due to the receiver's motion path.

To illustrate why this case must be excluded, consider a simplified scenario in which the receiver and SOP clocks are ideal, i.e., with no bias nor drift, such that the observations are given by $y(t_k) = \|\boldsymbol{r}_r(t_k) - \boldsymbol{r}_s(t_k)\|_2$. In this case, the state vector is given by $\boldsymbol{x} = [\boldsymbol{r}_r^\mathsf{T},\ \dot{\boldsymbol{r}}_r^\mathsf{T},\ \boldsymbol{r}_s^\mathsf{T}]^\mathsf{T}$, and the corresponding observability matrix is given by

$$\boldsymbol{\mathcal{O}}(t_0,t_l) = \begin{bmatrix} \mathbf{h}_{a,r,s}^\mathsf{T}(t_0) & \mathbf{0}_{1\times 2} & -\mathbf{h}_{a,r,s}^\mathsf{T}(t_0) \\ \mathbf{h}_{a,r,s}^\mathsf{T}(t_1) & T\mathbf{h}_{a,r,s}^\mathsf{T}(t_1) & -\mathbf{h}_{a,r,s}^\mathsf{T}(t_1) \\ \vdots & \vdots & \vdots \\ \mathbf{h}_{a,r,s}^\mathsf{T}(t_{l-1}) & T(l-1)\mathbf{h}_{a,r,s}^\mathsf{T}(t_{l-1}) & -\mathbf{h}_{a,r,s}^\mathsf{T}(t_{l-1}) \end{bmatrix}$$

where $\mathbf{h}_{a,r,s}^\mathsf{T}(t_k) \triangleq [(x_r(t_k) - x_s(t_k))/\|\boldsymbol{r}_r(t_k) - \boldsymbol{r}_s(t_k)\|_2,\ (y_r(t_k) - y_s(t_k))/\|\boldsymbol{r}_r(t_k) - \boldsymbol{r}_s(t_k)\|_2]$. An alternative expression for $\mathbf{h}_{a,r,s}^\mathsf{T}(t_k)$ is given by $\mathbf{h}_{a,r,s}^\mathsf{T}(t_k) = [\cos\theta_{r,s}(t_k),\ \sin\theta_{r,s}(t_k)]$, where $\theta_{r,s}(t_k)$ is the angle between the x-axis and the range vector connecting the receiver and the SOP at time instant t_k. In this representation, it is obvious that $\boldsymbol{\mathcal{O}}_L(t_0,t_l)$ has a rank of 3 since $\boldsymbol{\mathcal{O}}_1 = -\boldsymbol{\mathcal{O}}_5$, $\boldsymbol{\mathcal{O}}_2 = -\boldsymbol{\mathcal{O}}_6$, and $\sum_{i=1}^4 \alpha_i\ \boldsymbol{\mathcal{O}}_i = \mathbf{0}$, with $\alpha_1 \triangleq (-y_r(t_0) + y_s(t_0))/\dot{x}_r(t_0)$, $\alpha_2 \triangleq (x_r(t_0) - x_s(t_0))/\dot{x}_r(t_0)$, $\alpha_3 \triangleq (-\dot{y}_r(t_0)/\dot{x}_r(t_0))$, and $\alpha_4 \triangleq 1$, where $\boldsymbol{\mathcal{O}}_i$ is the ith column of $\boldsymbol{\mathcal{O}}_L(t_0,t_l)$. The null space of $\boldsymbol{\mathcal{O}}_L(t_0,t_l)$ for $l \geq 3$ can be shown to be

$$\mathcal{N}[\boldsymbol{\mathcal{O}}_L(t_0,t_l)] = \operatorname{span}[\,\boldsymbol{a}_1 \quad \boldsymbol{a}_2 \quad \boldsymbol{a}_3\,]$$
$$\boldsymbol{a}_1 \triangleq \boldsymbol{e}_1 + \boldsymbol{e}_5, \quad \boldsymbol{a}_2 \triangleq \boldsymbol{e}_2 + \boldsymbol{e}_6, \quad \boldsymbol{a}_3 \triangleq \sum_{i=1}^4 \alpha_i \boldsymbol{e}_i$$

where $\boldsymbol{e}_i$ is the standard basis vector consisting of a 1 in the ith element and zeros elsewhere. However, when the receiver's motion path is collinear with the SOP, the rank of $\boldsymbol{\mathcal{O}}_L(t_0,t_l)$ drops to 2 since, in this case, $\theta_{r,s}(t_0) = \cdots = \theta_{r,s}(t_{l-1})$.

C. Preliminary Facts

The following facts will be invoked in the upcoming proofs. The rank of an arbitrary matrix $\mathbf{A} \in \mathbb{R}^{m\times n}$ is the maximal number of linearly independent rows or columns; more specifically, $\operatorname{rank}[\mathbf{A}] \leq \min\{m,n\}$.

In a COpNav environment comprising n receivers and m SOPs, the state transition matrix raised to the kth power can be shown to be

$$\mathbf{F}^k = \operatorname{diag}\left[\mathbf{F}_{r_1}^k, \ldots, \mathbf{F}_{r_n}^k, \mathbf{F}_{s_1}^k, \ldots, \mathbf{F}_{s_m}^k\right] \tag{15}$$

where $\mathbf{F}_{r_i}$ and $\mathbf{F}_{s_j}$ are the state transition matrices for the ith receiver and jth SOP, respectively.

Moreover, it can be readily verified that

$$\boldsymbol{e}_i^\mathsf{T}\mathbf{F}_r^k = \begin{cases} \boldsymbol{e}_i^\mathsf{T} + kT\boldsymbol{e}_{i+2}^\mathsf{T}, & i = 1,2 \\ \boldsymbol{e}_i^\mathsf{T} + kT\boldsymbol{e}_{i+1}^\mathsf{T}, & i = 5 \\ \boldsymbol{e}_i^\mathsf{T}, & i = 3,4,6 \end{cases} \tag{16}$$

$$\boldsymbol{e}_i^\mathsf{T}\mathbf{F}_s^k = \begin{cases} \boldsymbol{e}_i^\mathsf{T}, & i = 1,2,4 \\ \boldsymbol{e}_i^\mathsf{T} + kT\boldsymbol{e}_{i+1}^\mathsf{T}, & i = 3. \end{cases} \tag{17}$$

The Jacobian vector of the observation corresponding to the pseudorange measurement made by receiver i on SOP j will have the following structure:

$$\begin{aligned} \mathbf{H}(t_k) &= \Big[\mathbf{0} \quad \cdots \quad \mathbf{0} \quad \mathbf{h}_{b,r_i,s_j}^\mathsf{T}(t_k) \quad \mathbf{0} \\ &\qquad \cdots \quad \mathbf{0} \quad \mathbf{h}_{c,r_i,s_j}^\mathsf{T}(t_k) \quad \mathbf{0} \quad \cdots \quad \mathbf{0}\Big] \\ \mathbf{h}_{b,r_i,s_j}^\mathsf{T}(t_k) &\triangleq \Big[\mathbf{h}_{a,r_i,s_j}^\mathsf{T}(t_k) \quad \mathbf{0}_{1\times 2} \quad c \quad 0\Big] \\ \mathbf{h}_{c,r_i,s_j}^\mathsf{T}(t_k) &\triangleq \Big[-\mathbf{h}_{a,r_i,s_j}^\mathsf{T}(t_k) \quad -c \quad 0\Big] \end{aligned} \tag{18}$$

where $\mathbf{h}_{a,r_i,s_j}^\mathsf{T}(t_k) = [(x_{r_i}(t_k) - x_{s_j}(t_k))/\|\boldsymbol{r}_{r_i}(t_k) - \boldsymbol{r}_{s_j}(t_k)\|_2,\ (y_{r_i}(t_k) - y_{s_j}(t_k))/\|\boldsymbol{r}_{r_i}(t_k) - \boldsymbol{r}_{s_j}(t_k)\|_2]$. It can be readily verified that

$$\mathbf{h}_{b,r_i,s_j}^\mathsf{T}(t_k)\mathbf{F}_r^k = \mathbf{h}_{d,r_i,s_j}^\mathsf{T}(t_k) \tag{19}$$

$$\begin{aligned} \mathbf{h}_{c,r_i,s_j}^\mathsf{T}(t_k)\mathbf{F}_s^k &= \mathbf{h}_{e,r_i,s_j}^\mathsf{T}(t_k) \\ \mathbf{h}_{d,r_i,s_j}^\mathsf{T}(t_k) &\triangleq [\,\mathbf{h}_{a,r_i,s_j}^\mathsf{T}(t_k) \quad kT\mathbf{h}_{a,r_i,s_j}^\mathsf{T}(t_k) \quad c \quad kT\,] \\ \mathbf{h}_{e,r_i,s_j}^\mathsf{T}(t_k) &\triangleq [\,-\mathbf{h}_{a,r_i,s_j}^\mathsf{T}(t_k) \quad -c \quad -kT\,]. \end{aligned} \tag{20}$$

TABLE I
COpNav OBSERVABILITY ANALYSIS SCENARIOS CONSIDERED

Case	Receiver(s)	SOP(s)
1	1 Unknown	1 Unknown
2	1 Unknown	m Partially-known
3	1 Unknown	1 Fully-known
4	1 Unknown	1 Fully-known & 1 Partially-known
5	n Partially-known	1 Unknown
6	n Partially-known	m Partially-known
7	1 Partially-known	1 Fully-known
8	1 Fully-known	1 Unknown

D. Scenarios Overview

The various scenarios considered are outlined in Table I. The first scenario corresponds to a single receiver and a single SOP whose initial states are unknown. (i.e., no *a priori* knowledge about any of the states is available). Subsequent scenarios consider cases of partial or full knowledge of the initial states. In Table I, fully known means that all the initial states are known. Thus, a fully known receiver is one with known $\boldsymbol{x}_r(t_0)$, whereas a fully known SOP is one with known $\boldsymbol{x}_s(t_0)$. On the other hand, partially known means that only the initial position states are known. Thus, a partially known receiver is one with known $\boldsymbol{r}_r(t_0)$, whereas a partially known SOP is one with known $\boldsymbol{r}_s(t_0)$. For the cases of multiple SOPs, it is assumed that the SOPs are not colocated at the same position. Moreover, it is assumed that the receivers identify the SOPs according to their classification: unknown, partially known, or fully known. The results associated with each case are captured in the following theorems and corresponding proofs.

E. Observability Analysis

Theorem IV.1: A COpNav environment with one unknown receiver and one unknown SOP is unobservable. Moreover, the observability matrix $\boldsymbol{\mathcal{O}}_L(t_0,t_l)$ is rank deficient by 5 $\forall\, l \geq 5$.

Proof: The state vector for this case is given by $\boldsymbol{x} = [\boldsymbol{x}_r^\mathsf{T},\ \boldsymbol{x}_s^\mathsf{T}]^\mathsf{T}$. Invoking (15), (18)–(20), it can be seen that the rank of $\boldsymbol{\mathcal{O}}_L(t_0,t_l)$ is one at the first time segment, and the rank increments by one as each additional time segment is appended up to $l=5$ since the corresponding additional rows are linearly independent. At the fifth time segment, rank$[\boldsymbol{\mathcal{O}}_L(t_0,t_5)] = 5$, and the rank never increases further since only $\boldsymbol{\mathcal{O}}_i$, $i=1,2,3,5,6$, are linearly independent $\forall l \geq 5$. This can be shown by noting that $\boldsymbol{\mathcal{O}}_1 = -\boldsymbol{\mathcal{O}}_7$, $\boldsymbol{\mathcal{O}}_2 = -\boldsymbol{\mathcal{O}}_8$, $\boldsymbol{\mathcal{O}}_5 = -\boldsymbol{\mathcal{O}}_9$, $\boldsymbol{\mathcal{O}}_6 = -\boldsymbol{\mathcal{O}}_{10}$, and $\sum_{i=1}^4 \alpha_i\ \boldsymbol{\mathcal{O}}_i = \boldsymbol{0}$, with $\alpha_1 \triangleq (-y_r(t_0) + y_s(t_0))/\dot{x}_r(t_0)$, $\alpha_2 \triangleq (x_r(t_0) - x_s(t_0))/\dot{x}_r(t_0)$, $\alpha_3 \triangleq (-\dot{y}_r(t_0))/\dot{x}_r(t_0)$, and $\alpha_4 \triangleq 1$. The null space of $\boldsymbol{\mathcal{O}}_L(t_0,t_l)$ for $l \geq 5$ can be shown to be

$$\mathcal{N}\left[\boldsymbol{\mathcal{O}}_L(t_0,t_l)\right] = \text{span}[\,\boldsymbol{n}_1 \quad \boldsymbol{n}_2 \quad \boldsymbol{n}_3 \quad \boldsymbol{n}_4 \quad \boldsymbol{n}_5\,]$$

$$\boldsymbol{n}_1 \triangleq \boldsymbol{e}_6 + \boldsymbol{e}_{10},\ \boldsymbol{n}_2 \triangleq \boldsymbol{e}_5 + \boldsymbol{e}_9,\ \boldsymbol{n}_3 \triangleq \boldsymbol{e}_2 + \boldsymbol{e}_8,\ \boldsymbol{n}_4 \triangleq \boldsymbol{e}_1 + \boldsymbol{e}_7$$

$$\boldsymbol{n}_5 \triangleq \alpha_1\boldsymbol{e}_1 + \alpha_2\boldsymbol{e}_2 + \alpha_3\boldsymbol{e}_3 + \alpha_4\boldsymbol{e}_4.$$

■

The structure of $\mathcal{N}[\boldsymbol{\mathcal{O}}_L(t_0,t_l)]$ reveals the following conclusions. First, the absence of a row of zeros in the matrix of null space basis vectors $\{\boldsymbol{n}_i\}_{i=1}^5$ indicates that none of the states is orthogonal to the unobservable subspace, which means that all the states lie within the unobservable subspace. Therefore, none of the states is directly observable. Second, a shift of the receiver and SOP positions by ε_x units in the x-direction and ε_y units in the y-direction, where $\varepsilon_x, \varepsilon_y \in \mathbb{R}$, is unobservable, since this shift, which is denoted $\boldsymbol{\lambda} = \varepsilon_y\boldsymbol{n}_3 + \varepsilon_x\boldsymbol{n}_4$, lies in the null space of $\boldsymbol{\mathcal{O}}_L(t_0,t_l)$. The same interpretation can be made with respect to a shift in the $\delta t - \dot{\delta} t$ space being unobservable as a result of $\boldsymbol{n}_1$ and $\boldsymbol{n}_2$. Third, a rotation by angle ϕ around the SOP is unobservable. To see this, without loss of generality, assume that the SOP is located at the origin. A rotation at an angle ϕ will transform the coordinate frame from (x,y) to (x',y'). Therefore, the position and velocity states in the new coordinate frame can be computed from

$$\begin{bmatrix} \boldsymbol{r}_r' \\ \dot{\boldsymbol{r}}_r' \end{bmatrix} = \begin{bmatrix} \mathbf{T}(\phi) & \boldsymbol{0} \\ \boldsymbol{0} & \mathbf{T}(\phi) \end{bmatrix} \begin{bmatrix} \boldsymbol{r}_r \\ \dot{\boldsymbol{r}}_r \end{bmatrix}\ \mathbf{T}(\phi) \triangleq \begin{bmatrix} \cos\phi & -\sin\phi \\ \sin\phi & \cos\phi \end{bmatrix}.$$

For small ϕ, the small angle approximations $\cos\phi \approx 1$ and $\sin\phi \approx \phi$ can be invoked in the rotation matrix $\mathbf{T}(\phi)$. Consequently, it can be readily shown that the transformed state vector can be expressed as $\boldsymbol{x}' = \boldsymbol{x} + (\phi/\dot{x}_r(t_0))\boldsymbol{n}_5$. Since $\boldsymbol{n}_5 \in \mathcal{N}[\boldsymbol{\mathcal{O}}_L(t_0,t_l)]$, then $(\phi/\dot{x}_r(t_0))\boldsymbol{n}_5 \in \mathcal{N}[\boldsymbol{\mathcal{O}}_L(t_0,t_l)]$, and such term will be unobservable from the measurements.

Theorem IV.2: A COpNav environment with one unknown receiver and m partially known SOPs is unobservable. Moreover, the observability matrix $\boldsymbol{\mathcal{O}}_L(t_0,t_l)$ is rank deficient by 3 for $m=1\ \forall\, l \geq 5$, and rank deficient by 2 for $m \geq 2\ \forall\, l \geq 4$.

Proof: The state vector for this case is given by $\boldsymbol{x} = [\boldsymbol{x}_r^\mathsf{T},\ \boldsymbol{x}_{s_1}^\mathsf{T}, \ldots, \boldsymbol{x}_{s_m}^\mathsf{T}]^\mathsf{T}$. Knowledge of the SOPs' positions is equivalent to having an observation Jacobian matrix of the form

$$\mathbf{H}(t_k) = \begin{bmatrix} \mathbf{h}_{b,r,s_1}^\mathsf{T}(t_k) & \mathbf{h}_{c,r,s_1}^\mathsf{T}(t_k) & \boldsymbol{0} & \cdots & \boldsymbol{0} \\ \mathbf{h}_{b,r,s_2}^\mathsf{T}(t_k) & \boldsymbol{0} & \mathbf{h}_{c,r,s_2}^\mathsf{T}(t_k) & \cdots & \boldsymbol{0} \\ \vdots & \vdots & \vdots & \ddots & \vdots \\ \mathbf{h}_{b,r,s_m}^\mathsf{T}(t_k) & \boldsymbol{0} & \boldsymbol{0} & \cdots & \mathbf{h}_{c,r,s_m}^\mathsf{T}(t_k) \\ \boldsymbol{0} & [\mathbf{I}_{2\times2}\ \boldsymbol{0}_{2\times2}] & \boldsymbol{0} & \cdots & \boldsymbol{0} \\ \boldsymbol{0} & \boldsymbol{0} & [\mathbf{I}_{2\times2}\ \boldsymbol{0}_{2\times2}] & \cdots & \boldsymbol{0} \\ \vdots & \vdots & \boldsymbol{0} & \ddots & \vdots \\ \boldsymbol{0} & \boldsymbol{0} & \boldsymbol{0} & \cdots & [\mathbf{I}_{2\times2}\ \boldsymbol{0}_{2\times2}] \end{bmatrix}.$$

Noting that $\mathbf{H}(t_k) \in \mathbb{R}^{(3m)\times(4m+6)}$ and invoking (15)–(20), it can be seen that rank$[\boldsymbol{\mathcal{O}}_L(t_0,t_1)] = 3m\ \forall m$ since all the rows are linearly independent. Adding a second time segment results in an observability matrix with rank$[\boldsymbol{\mathcal{O}}_L(t_0,t_2)] = 4m$ $\forall m$ since the first $4m$ rows are linearly independent, whereas rows $m+1,\ldots,3m$ are identical to rows $4m+1,\ldots,6m$, respectively. Adding a third time segment results in an observability matrix with

$$\text{rank}\left[\boldsymbol{\mathcal{O}}_L(t_0,t_3)\right] = \begin{cases} 5m, & m \leq 3 \\ 4m+4, & m > 3. \end{cases} \tag{21}$$

For $m \leq 3$, (21) can be shown by noting that rows $1, \ldots, 4m$ and $6m+i$, where $i = 1, 2, \ldots, m$ are linearly independent, whereas rows $m+1, \ldots, 3m$ are identical to rows $4m+1, \ldots, 6m$ and rows $7m+1, \ldots, 9m$, respectively. For $m > 3$, (21) can be shown by noting that columns $1, \ldots, 4m+4$ are linearly independent, whereas the last two columns are linearly dependent, namely, $\boldsymbol{\mathcal{O}}_{4m+5} = -\sum_{i=0}^{m-1} \boldsymbol{\mathcal{O}}_{4i+5}$ and $\boldsymbol{\mathcal{O}}_{4m+6} = -\sum_{i=0}^{m-1} \boldsymbol{\mathcal{O}}_{4i+6}$. Adding a fourth time segment results in an observability matrix with

$$\operatorname{rank}\left[\boldsymbol{\mathcal{O}}_L(t_0, t_4)\right] = \begin{cases} 6, & m = 1 \\ 4m+4, & m \geq 2. \end{cases} \tag{22}$$

For $m = 1$, (22) can be shown by noting that rows 1, 2, 3, 4, 7, and 10 are linearly independent, whereas rows $2+3i$ and $3+3i$ for $i = 0, 1, 2, 3$ are identical. For $m \geq 2$, (22) can be shown by noting that columns $1, \ldots, 4m+4$ are linearly independent, whereas the last two columns are linearly dependent, namely, $\boldsymbol{\mathcal{O}}_{4m+5} = -\sum_{i=0}^{m-1} \boldsymbol{\mathcal{O}}_{4i+5}$ and $\boldsymbol{\mathcal{O}}_{4m+6} = -\sum_{i=0}^{m-1} \boldsymbol{\mathcal{O}}_{4i+6}$. For $m \geq 2$, adding more time segments does not improve the rank any further as the last two columns will always be linearly dependent on the previous columns. However, for $m = 1$, a fifth time segment increases the rank by 1, whereas adding additional time segments beyond 5 does not improve the rank any further. This can be shown by noting that $\boldsymbol{\mathcal{O}}_i$, $i = 1, 2, 3, 5, 6, 7, 8$, are linearly independent, whereas $\boldsymbol{\mathcal{O}}_5 = -\boldsymbol{\mathcal{O}}_9$, $\boldsymbol{\mathcal{O}}_6 = -\boldsymbol{\mathcal{O}}_{10}$, and $\sum_{i=1}^{4} \alpha_i \, \boldsymbol{\mathcal{O}}_i = \mathbf{0}$.

For $m = 1$, the null space of $\boldsymbol{\mathcal{O}}_L(t_0, t_l)$, $l \geq 5$, can be shown to be

$$\mathcal{N}\left[\boldsymbol{\mathcal{O}}_L(t_0, t_l)\right] = \operatorname{span}[\, \boldsymbol{n}_1 \quad \boldsymbol{n}_2 \quad \boldsymbol{n}_5 \,].$$

For $m \geq 2$, the null space of $\boldsymbol{\mathcal{O}}_L(t_0, t_l)$, $l \geq 4$, can be shown to be

$$\begin{aligned} \mathcal{N}\left[\boldsymbol{\mathcal{O}}_L(t_0, t_l)\right] &= \operatorname{span}[\boldsymbol{n}_6 \quad \boldsymbol{n}_7] \\ \boldsymbol{n}_6 &\triangleq \begin{bmatrix} \boldsymbol{n}_{6,r}^{\mathsf{T}} & \boldsymbol{n}_{6,s_1}^{\mathsf{T}} & \boldsymbol{n}_{6,s_2}^{\mathsf{T}} & \cdots & \boldsymbol{n}_{6,s_m}^{\mathsf{T}} \end{bmatrix}^{\mathsf{T}} \\ \boldsymbol{n}_7 &\triangleq \begin{bmatrix} \boldsymbol{n}_{7,r}^{\mathsf{T}} & \boldsymbol{n}_{7,s_1}^{\mathsf{T}} & \boldsymbol{n}_{7,s_2}^{\mathsf{T}} & \cdots & \boldsymbol{n}_{7,s_m}^{\mathsf{T}} \end{bmatrix}^{\mathsf{T}} \\ \boldsymbol{n}_{6,r}^{\mathsf{T}} &\triangleq \gamma \boldsymbol{e}_5^{\mathsf{T}} - \mu \boldsymbol{e}_6^{\mathsf{T}}, \quad \boldsymbol{n}_{7,r}^{\mathsf{T}} \triangleq \mu \boldsymbol{e}_5^{\mathsf{T}} + \gamma \boldsymbol{e}_6^{\mathsf{T}} \\ \boldsymbol{n}_{6,s_i}^{\mathsf{T}} &\triangleq \gamma \boldsymbol{e}_3^{\mathsf{T}} - \mu \boldsymbol{e}_4^{\mathsf{T}} \\ \boldsymbol{n}_{7,s_i}^{\mathsf{T}} &\triangleq \mu \boldsymbol{e}_5^{\mathsf{T}} + \gamma \boldsymbol{e}_6^{\mathsf{T}}, \quad i = 1, 2, \ldots, m \\ \gamma &\triangleq \frac{-y_r(t_0) + \sum_{i=1}^{m} y_{s_i}(t_0)}{\dot{y}_r(t_0)} \\ \mu &\triangleq \frac{x_r(t_0) - \sum_{i=1}^{m} x_{s_i}(t_0)}{\dot{x}_r(t_0)}. \end{aligned}$$

The structure of $\mathcal{N}[\boldsymbol{\mathcal{O}}_L(t_0, t_l)]$ reveals that, for $m = 1$, none of the states is directly observable except x_{s_i} and y_{s_i}, which are observable by construction. However, for $m \geq 2$, the receiver's position and velocity states x_r, y_r, $\dot{x}_r$, and $\dot{y}_r$ become observable, but the receiver and SOPs clock bias and drift states δt_r, $\dot{\delta} t_r$, δt_{s_i}, and $\dot{\delta} t_{s_i}$ remain unobservable.

Theorem IV.3: A COpNav environment with one unknown receiver and one fully known SOP is unobservable. Moreover, the observability matrix $\boldsymbol{\mathcal{O}}_L(t_0, t_l)$ is rank deficient by $1 \; \forall \; l \geq 5$.

Proof: The state vector for this case is given by $\boldsymbol{x} = [\boldsymbol{x}_r^{\mathsf{T}}, \; \boldsymbol{x}_s^{\mathsf{T}}]^{\mathsf{T}}$. Full knowledge of the SOP is equivalent to having an observation Jacobian matrix of the form

$$\mathbf{H}(t_k) = \begin{bmatrix} \mathbf{h}_{b,r,s}^{\mathsf{T}}(t_k) & \mathbf{h}_{c,r,s}^{\mathsf{T}}(t_k) \\ \mathbf{0} & \mathbf{I}_{4\times 4} \end{bmatrix}. \tag{23}$$

Invoking (15)–(20), it can be seen that the observability matrix $\boldsymbol{\mathcal{O}}_L(t_0, t_l)$ has a rank of five at the first time segment since the rows are linearly independent. The rank increments by 1 as each additional time segment is appended up to $l = 5$ since rows 2, 3, 4, and 5 are identical to rows $2+5(l-1)$, $3+5(l-1)$, $4+5(l-1)$, and $5+5(l-1)$, respectively, whereas the first five rows are linearly independent of rows $1+5(l-1)$. The rank stops improving at the fifth time segment, whereat $\operatorname{rank}[\boldsymbol{\mathcal{O}}_L(t_0, t_5)] = 9$. The rank never increases further since $\boldsymbol{\mathcal{O}}_4 = -\sum_{i=1}^{3} \alpha_i \, \boldsymbol{\mathcal{O}}_i$. The null space of $\boldsymbol{\mathcal{O}}_L(t_0, t_l)$, $l \geq 5$ can be shown to be

$$\mathcal{N}\left[\boldsymbol{\mathcal{O}}_L(t_0, t_l)\right] = \operatorname{span}[\boldsymbol{n}_5].$$

■

The structure of $\mathcal{N}[\boldsymbol{\mathcal{O}}_L(t_0, t_l)]$ reveals that of the receiver's states, only the receiver clock bias δt_r and clock drift $\dot{\delta} t_r$ are observable as they are orthogonal to the unobservable subspace, whereas the SOP states are observable by construction.

Theorem IV.4: A COpNav environment with one unknown receiver, one fully known SOP, and one partially known SOP is observable $\forall \; l \geq 4$.

Proof: The state vector for this case is given by $\boldsymbol{x} = [\boldsymbol{x}_r^{\mathsf{T}}, \; \boldsymbol{x}_{s_1}^{\mathsf{T}}, \; \boldsymbol{x}_{s_2}^{\mathsf{T}}]^{\mathsf{T}}$. Full knowledge of one SOP and partial knowledge of the other is equivalent to having an observation Jacobian matrix of the form

$$\mathbf{H}(t_k) = \begin{bmatrix} \mathbf{h}_{b,r,s_1}^{\mathsf{T}}(t_k) & \mathbf{h}_{c,r,s_1}^{\mathsf{T}}(t_k) & \mathbf{0} \\ \mathbf{h}_{b,r,s_2}^{\mathsf{T}}(t_k) & \mathbf{0} & \mathbf{h}_{c,r,s_2}^{\mathsf{T}}(t_k) \\ \mathbf{0} & \mathbf{I}_{4\times 4} & \mathbf{0} \\ \mathbf{0} & \mathbf{0} & [\mathbf{I}_{2\times 2} \; \mathbf{0}_{2\times 2}] \end{bmatrix}. \tag{24}$$

Invoking (15)–(20), it can be seen that the observability matrix $\boldsymbol{\mathcal{O}}_L(t_0, t_l)$ has a rank of 8 at the first time segment since all the rows are linearly independent. The rank keeps incrementing by 2 as each additional time segment is appended up to $l = 4$. Adding a fourth time segment results in an observability matrix whose rank is 14 (full rank). This can be shown by noting that the first eight rows are linearly independent along with rows $9+8(l-2)$ and $10+8(l-2)$ for $l = 2, 3, 4$. Moreover, rows $i+8(l-1)$ for $i = 3, 4, 6, 7, 8$ and $l = 1$ are identical to the corresponding rows for $l = 2, 3, \ldots$. Finally, $\boldsymbol{\mathcal{O}}_{13+8(l-2)}^{\mathsf{T}} = \boldsymbol{\mathcal{O}}_5^{\mathsf{T}} + T(l-1)\boldsymbol{\mathcal{O}}_6^{\mathsf{T}}$ for $l = 2, 3, \ldots$, where $\boldsymbol{\mathcal{O}}_i^{\mathsf{T}}$ is the ith row of the corresponding observability matrix $\boldsymbol{\mathcal{O}}_L(t_0, t_l)$. ■

Theorem IV.5: A COpNav environment with n partially known receivers and one unknown SOP is unobservable. Moreover, the observability matrix $\boldsymbol{\mathcal{O}}_L(t_0, t_l)$ is rank deficient by $2 \; \forall \; l \geq 3$.

Proof: The state vector for this case is given by $\boldsymbol{x} = [\boldsymbol{x}_{r_1}^{\mathsf{T}}, \ldots, \boldsymbol{x}_{r_n}^{\mathsf{T}}, \; \boldsymbol{x}_s^{\mathsf{T}}]^{\mathsf{T}}$. Partial knowledge of the n receivers is

equivalent to having an observation Jacobian matrix of the form

$$\mathbf{H}(t_k)=\begin{bmatrix} \mathbf{h}^{\mathsf{T}}_{b,r_1,s}(t_k) & \mathbf{0} & \cdots & \mathbf{0} & \mathbf{h}^{\mathsf{T}}_{c,r_1,s}(t_k) \\ [\mathbf{I}_{2\times 2}\ \mathbf{0}_{2\times 4}] & \mathbf{0} & \cdots & \mathbf{0} & \mathbf{0} \\ \vdots & \vdots & \ddots & \vdots & \vdots \\ \mathbf{0} & \mathbf{0} & \cdots & \mathbf{h}^{\mathsf{T}}_{b,r_n,s}(t_k) & \mathbf{h}^{\mathsf{T}}_{c,r_n,s}(t_k) \\ \mathbf{0} & \mathbf{0} & \cdots & [\mathbf{I}_{2\times 2}\ \mathbf{0}_{2\times 4}] & \mathbf{0} \end{bmatrix}.$$

Noting that $\mathbf{H}(t_k)\in\mathbb{R}^{(3n)\times(6n+4)}$ and invoking (15)–(20), it can be seen that $\text{rank}[\boldsymbol{\mathcal{O}}_L(t_0,t_1)]=3n$ and $\text{rank}[\boldsymbol{\mathcal{O}}_L(t_0,t_2)]=6n$ since, in both cases, all rows are linearly independent. Adding more time segments results in $\text{rank}[\boldsymbol{\mathcal{O}}_L(t_0,t_l)]=6n+2,\ \forall\ l\geq 3$ since columns $1,2,\ldots,6n+2$ are linearly independent, whereas the last two columns are linearly dependent. In particular, $\boldsymbol{\mathcal{O}}_{6n+3}=-\sum_{i=1}^{n}\boldsymbol{\mathcal{O}}_{6i+5}$, and $\boldsymbol{\mathcal{O}}_{6n+4}=-\sum_{i=1}^{n}\boldsymbol{\mathcal{O}}_{6i+6}$. The null space of $\boldsymbol{\mathcal{O}}_L(t_0,t_l),\ l\geq 3$ can be shown to be

$$\begin{aligned}
\mathcal{N}[\boldsymbol{\mathcal{O}}_L(t_0,t_l)] &= \text{span}[\boldsymbol{n}_8 \quad \boldsymbol{n}_9] \\
\boldsymbol{n}_8 &\triangleq \begin{bmatrix}\boldsymbol{n}^{\mathsf{T}}_{8,r_1} & \boldsymbol{n}^{\mathsf{T}}_{8,r_2} & \cdots & \boldsymbol{n}^{\mathsf{T}}_{8,r_n} & \boldsymbol{n}^{\mathsf{T}}_{8,s}\end{bmatrix}^{\mathsf{T}} \\
\boldsymbol{n}_9 &\triangleq \begin{bmatrix}\boldsymbol{n}^{\mathsf{T}}_{9,r_1} & \boldsymbol{n}^{\mathsf{T}}_{9,r_2} & \cdots & \boldsymbol{n}^{\mathsf{T}}_{9,r_n} & \boldsymbol{n}^{\mathsf{T}}_{9,s}\end{bmatrix}^{\mathsf{T}} \\
\boldsymbol{n}^{\mathsf{T}}_{8,r_i} &\triangleq \xi\boldsymbol{e}^{\mathsf{T}}_5-\eta\boldsymbol{e}^{\mathsf{T}}_6, \\
\boldsymbol{n}^{\mathsf{T}}_{9,r_i} &\triangleq \eta\boldsymbol{e}^{\mathsf{T}}_5+\xi\boldsymbol{e}^{\mathsf{T}}_6, \quad i=1,2,\ldots,n \\
\boldsymbol{n}^{\mathsf{T}}_{8,s} &\triangleq \xi\boldsymbol{e}^{\mathsf{T}}_3-\eta\boldsymbol{e}^{\mathsf{T}}_4, \quad \boldsymbol{n}^{\mathsf{T}}_{9,s}\triangleq\eta\boldsymbol{e}^{\mathsf{T}}_3+\xi\boldsymbol{e}^{\mathsf{T}}_4 \\
\xi &\triangleq \frac{-[\sum_{i=1}^{n}y_{r_i}(t_0)]+y_s(t_0)}{\sum_{i=1}^{n}\dot{y}_{r_i}(t_0)} \\
\eta &\triangleq \frac{[\sum_{i=1}^{n}x_{r_i}(t_0)]-x_s(t_0)}{\sum_{i=1}^{n}\dot{x}_{r_i}(t_0)}.
\end{aligned}$$

The structure of $\mathcal{N}[\boldsymbol{\mathcal{O}}_L(t_0,t_l)]$ reveals that the receivers velocity states and the SOP's position states are observable. However, the receivers' and the SOP's clock bias and drift states are not observable. Recall that the receivers' position states are observable by construction.

Theorem IV.6: A COpNav environment with n partially known receivers and m partially known SOPs is unobservable. Moreover, the observability matrix $\boldsymbol{\mathcal{O}}_L(t_0,t_l)$ is rank deficient by $2\ \forall\ l\geq 2$.

Proof: The state vector for this case is given by $\boldsymbol{x}=[\boldsymbol{x}^{\mathsf{T}}_{r_1},\ldots,\boldsymbol{x}^{\mathsf{T}}_{r_n},\ \boldsymbol{x}^{\mathsf{T}}_{s_1},\ldots,\boldsymbol{x}^{\mathsf{T}}_{s_m}]^{\mathsf{T}}$. Partial knowledge of the receivers and SOPs is equivalent to having an observation Jacobian matrix of the form

$$\begin{aligned}
&\mathbf{H}(t_k) \\
&=\begin{bmatrix} \mathbf{H}_{b,r_1,s} & \mathbf{0} & \mathbf{0} & \mathbf{H}_{c,r_1,s} & \mathbf{0} & \mathbf{0} \\ \mathbf{0} & \ddots & \vdots & \mathbf{0} & \ddots & \mathbf{0} \\ \mathbf{0} & \cdots & \mathbf{H}_{b,r_n,s} & \mathbf{0} & \cdots & \mathbf{H}_{c,r_n,s} \\ \mathbf{0} & \cdots & \mathbf{0} & [\mathbf{I}_{2\times 2}\ \mathbf{0}_{2\times 2}] & \mathbf{0} & \mathbf{0} \\ \vdots & \ddots & \vdots & \mathbf{0} & \ddots & \vdots \\ \mathbf{0} & \cdots & \mathbf{0} & \mathbf{0} & \cdots & [\mathbf{I}_{2\times 2}\ \mathbf{0}_{2\times 2}] \end{bmatrix}
\end{aligned}$$

$$\mathbf{H}_{b,r_i,s}(t_k)\triangleq\begin{bmatrix}\mathbf{h}^{\mathsf{T}}_{b,r_i,s_1}(t_k)\\ \vdots \\ \mathbf{h}^{\mathsf{T}}_{b,r_i,s_m}(t_k)\\ \mathbf{I}_{2\times 2}\ \mathbf{0}_{2\times 4}\end{bmatrix},\quad i=1,\ldots,n$$

$$\mathbf{H}_{c,r_i,s}(t_k)\triangleq\begin{bmatrix}\mathbf{h}^{\mathsf{T}}_{c,r_i,s_1}(t_k)\\ \vdots \\ \mathbf{h}^{\mathsf{T}}_{c,r_i,s_m}(t_k)\\ \mathbf{0}_{2\times 4}\end{bmatrix},\quad i=1,\ldots,n.$$

Noting that $\mathbf{H}(t_k)\in\mathbb{R}^{(mn+2n+2m)\times(6n+4m)}$ and invoking (15)–(20), it can be seen that $\text{rank}[\boldsymbol{\mathcal{O}}_L(t_0,t_1)]=3n+3m-1$. This can be shown by noting that the columns of $\boldsymbol{\mathcal{O}}(t_0,t_1)$ have the following properties.

1) Linearly independent columns: $\boldsymbol{\mathcal{O}}_{1+6i}$, $\boldsymbol{\mathcal{O}}_{2+6i}$, $\boldsymbol{\mathcal{O}}_{5+6i}$, $\boldsymbol{\mathcal{O}}_{6n+1+4j}$, $\boldsymbol{\mathcal{O}}_{6n+2+4j}$, and $\boldsymbol{\mathcal{O}}_{6n+3+4(l-1)}$, with $i=0,1,\ldots,n$, $j=0,1,\ldots,m$, and $l=1,2,\ldots,j$.
2) Columns of zeros: $\boldsymbol{\mathcal{O}}_{3+6i}$, $\boldsymbol{\mathcal{O}}_{4+6i}$, $\boldsymbol{\mathcal{O}}_{6+6i}$, and $\boldsymbol{\mathcal{O}}_{6n+4+4j}$, with $i=0,1,\ldots,n$ and $j=0,1,\ldots,m$.
3) Linearly dependent columns: $\boldsymbol{\mathcal{O}}_{6n+3+4j}=-[\sum_{l=1}^{n}\boldsymbol{\mathcal{O}}_{6l-1}+\sum_{l=0}^{j-1}\boldsymbol{\mathcal{O}}_{6n+3+4l}]$, with $j=0,\ldots,m$.

Next, it is noted that $\boldsymbol{\mathcal{O}}_L(t_0,t_l)\in\mathbb{R}^{[l(mn+2n+2m)]\times(6n+4m)}$; hence, the rank of $\boldsymbol{\mathcal{O}}_L(t_0,t_l)$ will be determined by the number of linearly independent columns since the matrix will have more rows than columns $\forall l\geq 2$. It can be seen that $\text{rank}[\boldsymbol{\mathcal{O}}_L(t_0,t_l)]=6n+4m-2\ \forall l\geq 2$, i.e., the l-step observability matrix is rank deficient by 2. This can be shown by noting that the first $6n+4m-2$ columns are linearly independent, whereas the last two columns are linearly dependent, such that

$$\boldsymbol{\mathcal{O}}_{6n+4m-q}=-\left[\sum_{l=1}^{n}\boldsymbol{\mathcal{O}}_{6l-q}+\sum_{l=0}^{j-1}\boldsymbol{\mathcal{O}}_{6n+4-q+4l}\right]$$

where $q=0,1$ and $j=0,1,\ldots,m$. The null space of $\boldsymbol{\mathcal{O}}_L(t_0,t_l),\ l\geq 3$, can be shown to be

$$\begin{aligned}
\mathcal{N}[\boldsymbol{\mathcal{O}}_L(t_0,t_l)] &= \text{span}[\boldsymbol{n}_{10} \quad \boldsymbol{n}_{11}] \\
\boldsymbol{n}_{10} &\triangleq \begin{bmatrix}\boldsymbol{n}^{\mathsf{T}}_{10,r_1} & \cdots & \boldsymbol{n}^{\mathsf{T}}_{10,r_n} & \boldsymbol{n}^{\mathsf{T}}_{10,s_1} & \cdots & \boldsymbol{n}^{\mathsf{T}}_{10,s_m}\end{bmatrix}^{\mathsf{T}} \\
\boldsymbol{n}_{11} &\triangleq \begin{bmatrix}\boldsymbol{n}^{\mathsf{T}}_{11,r_1} & \cdots & \boldsymbol{n}^{\mathsf{T}}_{11,r_n} & \boldsymbol{n}^{\mathsf{T}}_{11,s_1} & \cdots & \boldsymbol{n}^{\mathsf{T}}_{11,s_m}\end{bmatrix}^{\mathsf{T}} \\
\boldsymbol{n}^{\mathsf{T}}_{10,r_i} &\triangleq \beta\boldsymbol{e}^{\mathsf{T}}_5-\zeta\boldsymbol{e}^{\mathsf{T}}_6, \quad \boldsymbol{n}^{\mathsf{T}}_{9,r_i}\triangleq\zeta\boldsymbol{e}^{\mathsf{T}}_5+\beta\boldsymbol{e}^{\mathsf{T}}_6, \quad i=1,2,\ldots,n \\
\boldsymbol{n}^{\mathsf{T}}_{11,s_j} &\triangleq \beta\boldsymbol{e}^{\mathsf{T}}_3-\zeta\boldsymbol{e}^{\mathsf{T}}_4, \quad \boldsymbol{n}^{\mathsf{T}}_{9,s_j}\triangleq\zeta\boldsymbol{e}^{\mathsf{T}}_3+\beta\boldsymbol{e}^{\mathsf{T}}_4, \quad j=1,2,\ldots,m \\
\beta &\triangleq \frac{-[\sum_{i=1}^{n}y_{r_i}(t_0)]+\left[\sum_{j=1}^{m}y_{s_i}(t_0)\right]}{\sum_{i=1}^{n}\dot{y}_{r_i}(t_0)} \\
\zeta &\triangleq \frac{[\sum_{i=1}^{n}x_{r_i}(t_0)]-\left[\sum_{j=1}^{m}x_{s_i}(t_0)\right]}{\sum_{i=1}^{n}\dot{x}_{r_i}(t_0)}.
\end{aligned}$$

The structure of $\mathcal{N}[\boldsymbol{\mathcal{O}}_L(t_0,t_l)]$ reveals that the receivers velocity states are observable. However, the receivers' and SOPs' clock bias and drift states are not observable. Recall that the receivers' position states are observable by construction.

TABLE II
COPNAV OBSERVABILITY ANALYSIS RESULTS

Case	Observable?	Observable States	Time Step l
1	no	none	5
2	no	$m = 1$: none $m \geq 2$: x_r, y_r, $\dot{x}_r$, $\dot{y}_r$	5 4
3	no	δt_r, $\dot{\delta t}_r$	5
4	yes	all	4
5	no	$\dot{x}_{r_i}$, $\dot{y}_{r_i}$, x_s, y_s, $i = 1, \ldots, n$	3
6	no	$\dot{x}_{r_i}$, $\dot{y}_{r_i}$, $i = 1, \ldots, n$	2
7	yes	all	2
8	yes	all	4

Theorem IV.7: A COpNav environment with one partially known receiver and one fully known SOP is observable $\forall\, l \geq 2$.

Proof: The state vector for this case is given by $\boldsymbol{x} = [\boldsymbol{x}_r^\mathsf{T},\ \boldsymbol{x}_s^\mathsf{T}]^\mathsf{T}$. Partial knowledge of the receiver and full knowledge of the SOP is equivalent to having an observation Jacobian matrix of the form

$$\mathbf{H}(t_k) = \begin{bmatrix} \mathbf{h}_{b,r,s}^\mathsf{T}(t_k) & \mathbf{h}_{c,r,s}^\mathsf{T}(t_k) \\ [\mathbf{I}_{2\times 2}\ \mathbf{0}_{2\times 4}] & \mathbf{0} \\ \mathbf{0} & \mathbf{I}_{4\times 4} \end{bmatrix}. \tag{25}$$

Invoking (15)–(20), it can be seen that $\text{rank}[\boldsymbol{\mathcal{O}}_L(t_0, t_1)] = 7$ since all the rows are linearly independent. Adding more time segments yields $\text{rank}[\boldsymbol{\mathcal{O}}_L(t_0, t_1)] = 10$ (full rank) $\forall l \geq 2$ since the first ten rows are linearly independent, whereas rows $4 + 7(l-1)$, $5 + 7(l-1)$, and $7 + 7(l-1)$ for $l = 1$ are identical to the corresponding rows for $l = 2, 3, \ldots$, and rows $\boldsymbol{\mathcal{O}}_{6+7(l-1)}^\mathsf{T}$ are linearly dependent, such that $\boldsymbol{\mathcal{O}}_{6+7(l-1)}^\mathsf{T} = \boldsymbol{\mathcal{O}}_6^\mathsf{T} + T(l-1)\boldsymbol{\mathcal{O}}_7^\mathsf{T}$. ■

Theorem IV.8: A COpNav environment with one fully known receiver and one unknown SOP is observable $\forall\, l \geq 4$.

Proof: The state vector for this case is given by $\boldsymbol{x} = [\boldsymbol{x}_r^\mathsf{T},\ \boldsymbol{x}_s^\mathsf{T}]^\mathsf{T}$. Full knowledge of the receiver is equivalent to having an observation Jacobian matrix of the form

$$\mathbf{H}(t_k) = \begin{bmatrix} \mathbf{h}_{b,r,s}^\mathsf{T}(t_k) & \mathbf{h}_{c,r,s}^\mathsf{T}(t_k) \\ \mathbf{I}_{6\times 6} & \mathbf{0} \end{bmatrix}. \tag{26}$$

Invoking (15)–(20), it can be seen that the observability matrix $\boldsymbol{\mathcal{O}}_L(t_0, t_l)$ has a rank of 7 at the first time segment since all the rows are linearly independent. The rank increments by one as each additional segment is appended up to $l = 4$. Adding a fourth time segment results in an observability matrix whose rank is 10 (full rank). This can be shown by noting that the first seven rows are linearly independent along with rows $8 + 7(l-2)$ for $l = 2, 3, 4$. Moreover, rows $i + 7(l-1)$ for $i = 4, 5, 7$ and $l = 1, 2, \ldots$, are identical, respectively. Finally, $\boldsymbol{\mathcal{O}}_{9+7(l-2)}^\mathsf{T} = \boldsymbol{\mathcal{O}}_2^\mathsf{T} + T(l-1)\boldsymbol{\mathcal{O}}_4^\mathsf{T}$, $\boldsymbol{\mathcal{O}}_{10+7(l-2)}^\mathsf{T} = \boldsymbol{\mathcal{O}}_3^\mathsf{T} + T(l-1)\boldsymbol{\mathcal{O}}_5^\mathsf{T}$, and $\boldsymbol{\mathcal{O}}_{13+7(l-2)}^\mathsf{T} = \boldsymbol{\mathcal{O}}_6^\mathsf{T} + T(l-1)\boldsymbol{\mathcal{O}}_7^\mathsf{T}$ for $l = 2, 3, \ldots$. ■

The results concluded from Theorems IV.1–IV.8 are summarized in Table II, where observable states refer to those in an orthogonal complement to the unobservable subspace, and time step l refers to the time step at which the observability matrix rank reaches a steady-state value. It is worth noting that the observability results for the scenarios considered in Table I constitute the minimal set of observability requirements in the sense that, by knowing the results for these scenarios, one can predict the observability of an arbitrary scenario with n receivers and m SOPs and any type of prior knowledge (none, partial, or full) for the receivers and SOPs.

V. SIMULATION RESULTS

Here, simulation results are presented, which were achieved for the three observable cases in Table I: Cases 4, 7, and 8. For purposes of numerical stability, the clock error states were defined to be $c\delta t$ and $c\dot{\delta t}$. All simulations assumed the receiver's process noise spectral density to be $\tilde{q}_x = \tilde{q}_y = 0.1\ \text{m}^2/\text{s}^4$, whereas the sampling period was set to $T = 10$ ms. The receiver's clock was assumed to be a temperature-compensated crystal oscillator with $h_0 = 2 \times 10^{-19}$ and $h_{-2} = 2 \times 10^{-20}$, whereas the SOPs' clocks were assumed to be oven-controlled crystal oscillators with $h_0 = 8 \times 10^{-20}$ and $h_{-2} = 4 \times 10^{-23}$. The observation noise spectral density was set to $r = 100\ \text{m}^2$.

A simulator was developed to generate the "truth" data for each COpNav environment studied. Noisy pseudorange observations were processed by an EKF to estimate the states of interest. The observability is quantified in terms of the estimation error $\tilde{\boldsymbol{x}} \triangleq \boldsymbol{x} - \hat{\boldsymbol{x}}$ and the corresponding estimation error covariance $\mathbf{P} \triangleq \mathbb{E}[\tilde{\boldsymbol{x}}\, \tilde{\boldsymbol{x}}^\mathsf{T}]$, where $\hat{\boldsymbol{x}}$ is the EKF state estimate. Results for a single-run EKF and rigorous MC analysis are presented. The MC analysis is based on an N-run average of the normalized estimation error squared (NEES) [31]. The ith-run NEES is defined as $\epsilon_i(t_k) \triangleq \tilde{\boldsymbol{x}}_i^\mathsf{T}(t_k|t_k)\mathbf{P}_i^{-1}(t_k|t_k)\tilde{\boldsymbol{x}}_i(t_k|t_k)$, whereas the average NEES is defined as $\bar{\epsilon}(t_k) = 1/N \sum_{i=1}^{N} \epsilon_i(t_k)$. For the single-run EKF, an observable system should yield converging estimation error covariances, and the estimation errors should remain bounded. For the N-run EKF, an observable system and a consistent EKF should yield a statistic $N\bar{\epsilon}(t_k)$ that is approximately chi-squared distributed with Nn degrees of freedom, specifically $N\bar{\epsilon}(k) \sim \chi^2_{Nn}$, where n is the state estimate dimension. An unobservable system should yield an estimation error covariance that never improves with more observations. Thus, the MC analysis boils down to a hypothesis test on $\bar{\epsilon}(t_k)$ with an acceptance region $[r_1, r_2]$ defined such that $\Pr\{\bar{\epsilon}(k) \in [r_1, r_2] | H_0\} = 1 - \alpha$, where H_0 is the null hypothesis, and α is the size of the test (probability of false alarm).

In the following simulations, the system true initial state $\boldsymbol{x}(t_0|t_{-1})$ was fixed, whereas the EKF initial state estimate $\hat{\boldsymbol{x}}(t_0)$ was generated according to $\hat{\boldsymbol{x}}(t_0|t_{-1}) \sim \mathcal{N}[\boldsymbol{x}(t_0), \mathbf{P}(t_0|t_{-1})]$, where $\mathbf{P}(t_0|t_{-1})$ is the EKF initial estimation error covariance. All the simulations assumed a receiver whose initial state is $\boldsymbol{x}_r(t_0) = [0, 0, 0, 25, 10, 1]^\mathsf{T}$ and SOPs with initial states $\boldsymbol{x}_{s_1}(t_0) = [50, 100, 1, 0.1]^\mathsf{T}$ and $\boldsymbol{x}_{s_2}(t_0) = [-50, 100, 1, 0.1]^\mathsf{T}$.

The simulations for Case 4 considered an environment with an unknown receiver and two SOPs: one fully known and one partially known. The initial estimation error covariance matrices of the receiver and the second SOP were chosen to be $\mathbf{P}_r(t_0|t_{-1}) = (1 \times 10^3)\text{diag}[2, 2, 1, 1, 30, 0.3]$ and $\mathbf{P}_{s_2}(t_0|t_{-1}) = (1 \times 10^3)\text{diag}[30, 0.3]$, respectively.

The simulations for Case 7 considered an environment with a partially known receiver and two SOPs: one fully known

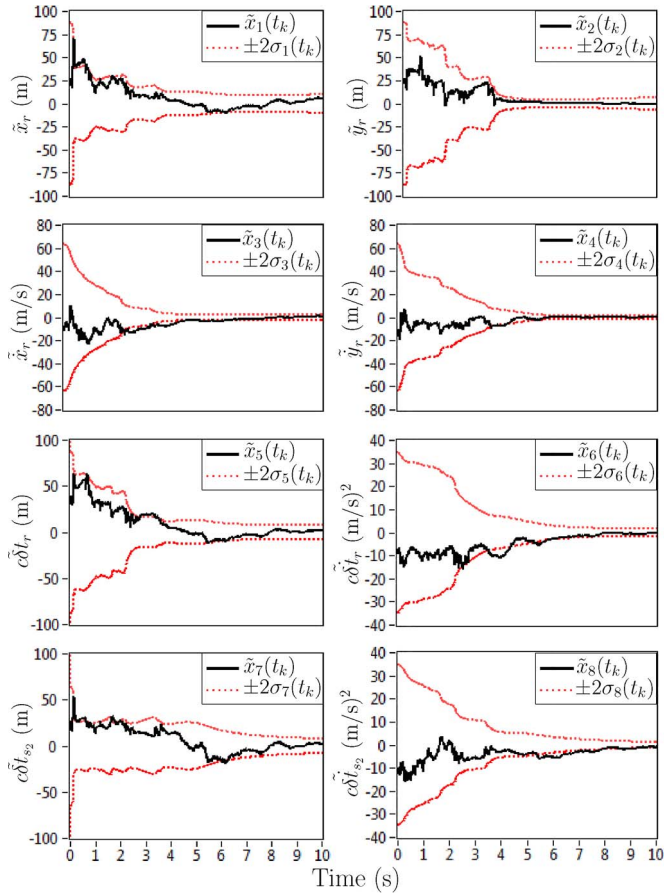

Fig. 1. Estimation error trajectories and $\pm 2\sigma$ bounds for Case 4 in Table I.

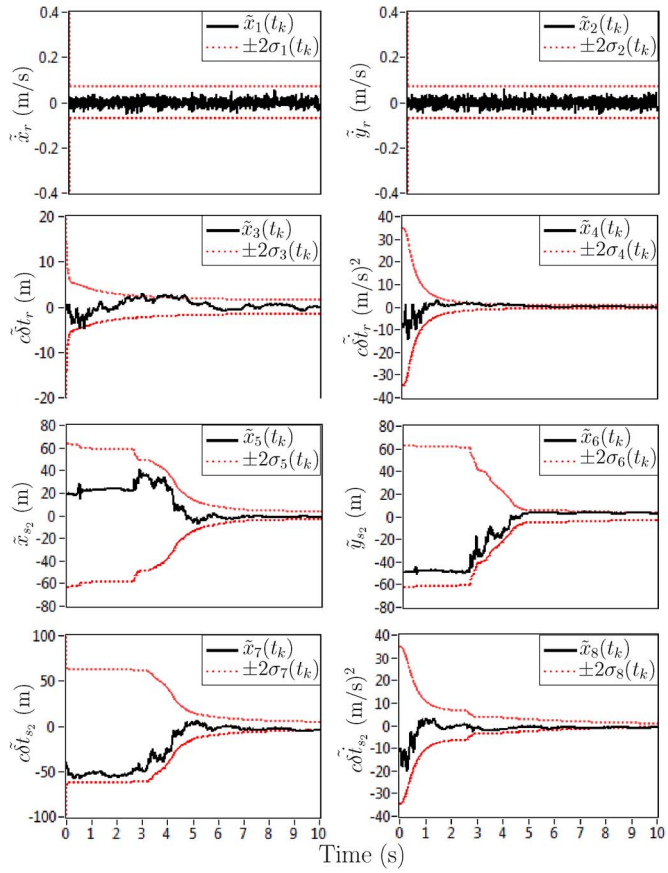

Fig. 2. Estimation error trajectories and $\pm 2\sigma$ bounds for Case 7 in Table I.

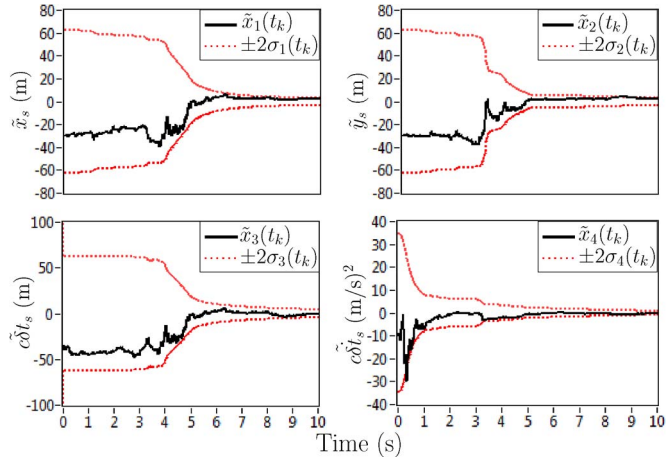

Fig. 3. Estimation error trajectories and $\pm 2\sigma$ bounds for Case 8 in Table I.

and one unknown. The initial estimation error covariance matrices of the receiver and the second SOP were chosen to be $\mathbf{P}_r(t_0|t_{-1}) = (1 \times 10^3)\text{diag}[1, 1, 30, 0.3]$ and $\mathbf{P}_{s_2}(t_0|t_{-1}) = (1 \times 10^3)\text{diag}[1, 1, 30, 0.3]$, respectively.

The simulations for Case 8 considered an environment with a fully known receiver and one unknown SOP. The initial estimation error covariance matrix of the SOP was chosen to be $\mathbf{P}_{s_1}(t_0|t_{-1}) = (1 \times 10^3)\text{diag}[1, 1, 30, 0.3]$.

Figs. 1–3 show the estimation error trajectories $\tilde{x}_i(t_k|t_k)$ for a single-run EKF along with the $\pm 2\sigma_i(t_k|t_k)$ estimation error variance bounds for Cases 4, 7, and 8, respectively. Note that the estimation error variances converge and that the estimation errors remain bounded as would be expected for an observable system.

Figs. 4–6 show the resulting NEES trajectories $\bar{\epsilon}(t_k)$ for $\alpha = 0.01$ along with r_1 and r_2 for Cases 4, 7, and 8, respectively. Note that the $\bar{\epsilon}(t_k)$ values reside within the 99% probability region, which is consistent with a well-behaved estimator operating on an observable system.

VI. Experimental Results

A field experimental demonstration was conducted to illustrate one of the observable cases in Table I, namely, Case 8. The objective was to demonstrate that a COpNav receiver with velocity random-walk dynamics and knowledge of its initial state can estimate the states of an unknown SOP in its environment. To this end, two antennas were mounted on a vehicle to acquire and track: 1) multiple GPS signals; and 2) a signal from a nearby cellular phone tower whose signal was modulated through code-division multiple access (CDMA). The GPS and cellular signals were simultaneously downmixed and synchronously sampled via two National Instruments vector RF signal analyzers. These front ends fed their data to a Generalized Radionavigation Interfusion Device (GRID) software receiver [42], which simultaneously tracked all GPS L1 C/A signals in view and the signal from the cellular tower with unknown states, producing pseudorange observables for

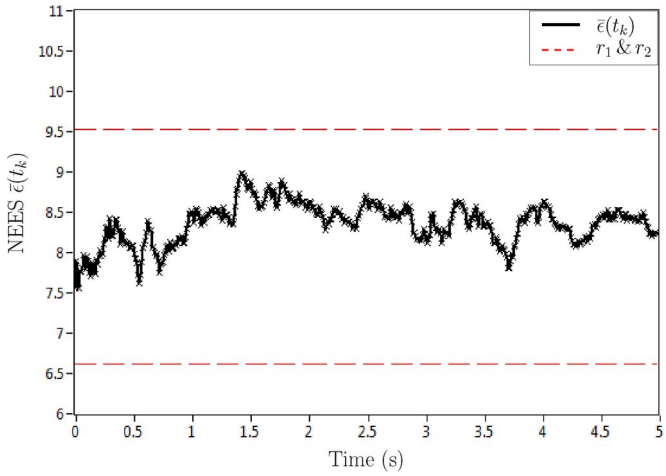

Fig. 4. NEES and r_1 and r_2 bounds for Case 4 in Table I with 50 MC runs.

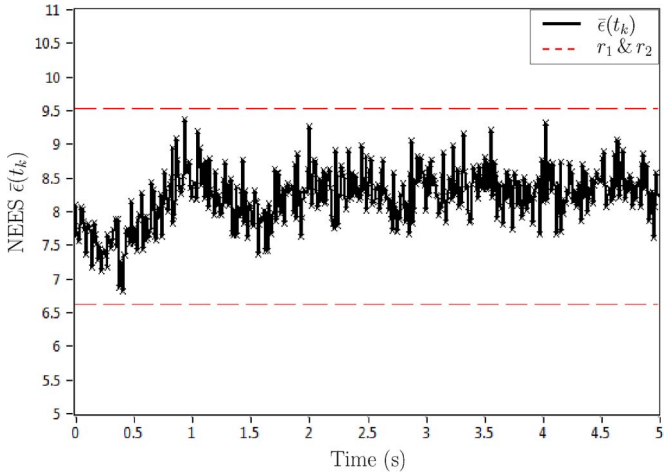

Fig. 5. NEES and r_1 and r_2 bounds for Case 7 in Table I with 50 MC runs.

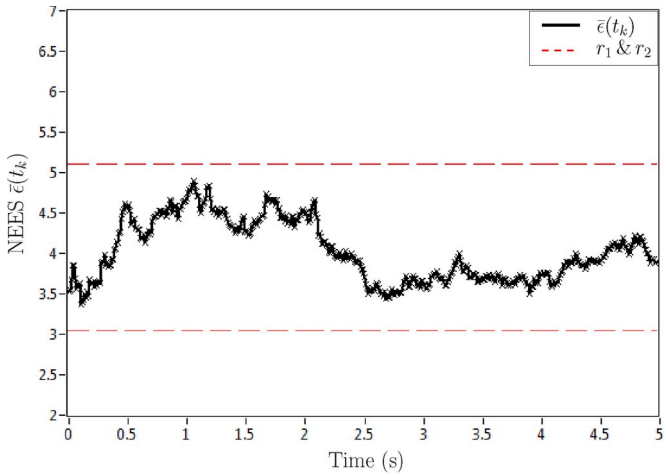

Fig. 6. NEES and r_1 and r_2 bounds for Case 8 in Table I with 50 MC runs.

all tracked signals. The observables were fed into a MATLAB-based EKF, which estimated the states of the unknown CDMA cellular tower. Fig. 7 shows the hardware setup of the conducted experiment.

Since the states of the GPS satellite vehicles (SVs) were known, and since the receiver was tracking more than four GPS SVs throughout the experiment, the receiver's initial state

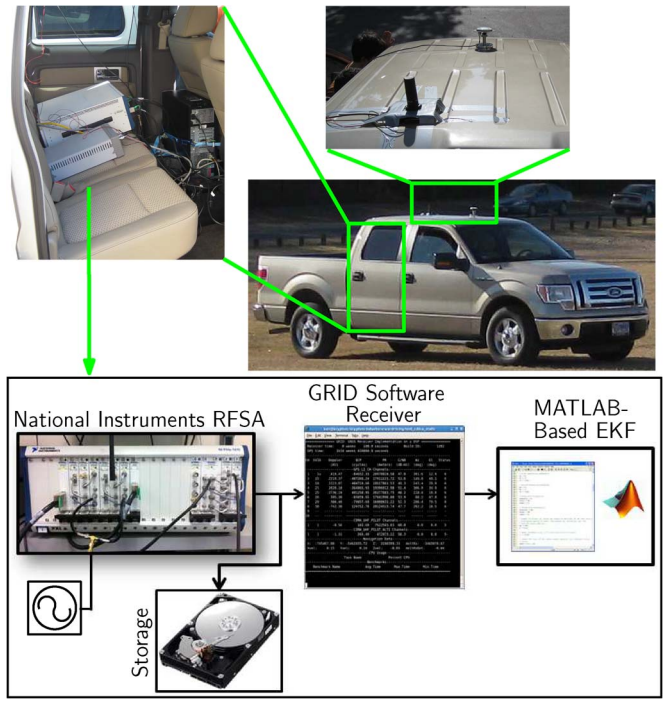

Fig. 7. Experiment hardware setup.

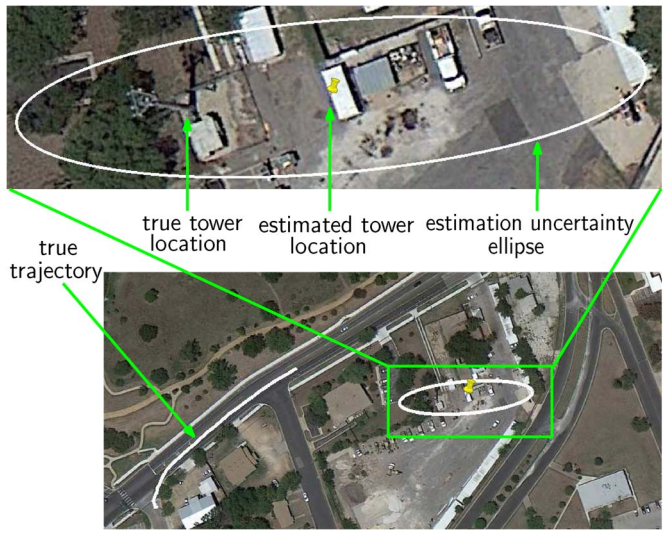

Fig. 8. Vehicle traversed trajectory during the collection of the GPS and cellular CDMA observations, true location of cellular CDMA tower, and estimated CDMA tower location and associated estimation error ellipse.

$\boldsymbol{x}_r(t_0)$ was fully known. The cellular tower state vector consisted of its planar position states, clock bias, and clock drift, as defined in (7). The EKF initial state estimate $\hat{\boldsymbol{x}}(t_0|t_{-1})$ was generated according to $\hat{\boldsymbol{x}}(t_0|t_{-1}) \sim \mathcal{N}[\boldsymbol{x}(t_0), \mathbf{P}(t_0|t_{-1})]$, where $\boldsymbol{x}(t_0) \triangleq [\boldsymbol{r}_s^{\mathsf{T}}(t_0), c\delta t_s(t_0), 0]^{\mathsf{T}}$, where $\boldsymbol{r}_s^{\mathsf{T}} \triangleq [x_s(t_0), y_s(t_0)]$ is the projection of the true cellular tower location from the Earth-Centered Earth-Fixed (ECEF) coordinate frame system to a planar system, $c\delta t_s(t_0) = \|\boldsymbol{r}_r(t_0) - \hat{\boldsymbol{r}}_s(t_0|t_{-1})\|_2 - \rho(t_0) + c\delta t_r(t_0)$, $\boldsymbol{r}_r^{\mathsf{T}}(t_0) \triangleq [x_r(t_0), y_r(t_0)]$ is the planar projection of the receiver's initial location from ECEF, and $\mathbf{P}(t_0|t_{-1}) = \text{diag}[1\times10^4, 1\times10^4, 3\times10^4, 3\times10^2]$ is the EKF initial estimation error covariance matrix. Fig. 8 shows the receiver traversed trajectory during the collection of the pseudorange

observations, the true and estimated location of the cellular phone tower, and the uncertainty ellipse produced by the EKF estimation error covariance. Despite the short COpNav receiver trajectory, the tower location estimate was within about 10 m of the actual tower and within the estimation uncertainty ellipse. This result is consistent with the theoretical prediction that a COpNav receiver with a fully known initial state can estimate the states of an unknown SOP.

VII. Conclusion

This paper has addressed one component of a fundamental theory of COpNav, namely, observability of the environment. A set of building block planar COpNav scenarios was considered, and the observability of each scenario was analyzed. It was concluded that a planar COpNav environment consisting of multiple receivers with velocity random-walk dynamics making pseudorange measurements on multiple stationary SOPs is fully observable if and only if the initial state(s) of: 1) at least one receiver is fully known, 2) at least one receiver is partially known and at least one SOP is fully known, or 3) at least one SOP is fully known and at least one SOP is partially known. Aided by this observability analysis, future work will consider prescribing receiver trajectories that will maximize the estimability of states of interest in the COpNav environment.

Acknowledgment

The authors would like to thank Prof. A. Arapostathis for his feedback and helpful discussions that have added value to this research and the members of the Radionavigation Laboratory for their assistance with the data collection of the experiment.

References

[1] S. Saab and Z. Kassas, "Map-based land vehicle navigation system with DGPS," in *Proc. IEEE Intell. Veh. Symp.*, Jun. 2002, vol. 1, pp. 209–214.
[2] S. Saab and Z. Kassas, "Power matching approach for GPS coverage extension," *IEEE Trans. Intell. Transp. Syst.*, vol. 7, no. 2, pp. 156–166, Jun. 2006.
[3] R. Toledo-Moreo, M. Zamora-Izquierdo, B. Ubeda-Miarro, and A. Gomez-skarmeta, "High-integrity IMM-EKF-based road vehicle navigation with low-cost GPS/SBAS/INS," *IEEE Trans. Intell. Transp. Syst.*, vol. 8, no. 3, pp. 491–511, Sep. 2007.
[4] I. Skog and P. Handel, "In-car positioning and navigation technologies—A survey," *IEEE Trans. Intell. Transp. Syst.*, vol. 10, no. 1, pp. 4–21, Mar. 2009.
[5] A. Ramanandan, A. Chen, and J. Farrell, "Inertial navigation aiding by stationary updates," *IEEE Trans. Intell. Transp. Syst.*, vol. 13, no. 1, pp. 235–248, Mar. 2012.
[6] K. Pesyna, Z. Kassas, J. Bhatti, and T. Humphreys, "Tightly-coupled opportunistic navigation for deep urban and indoor positioning," in *Proc. ION GNSS*, Sep. 2011, vol. 1, pp. 3605–3617.
[7] Z. Kassas, "Collaborative opportunistic navigation," *IEEE Aerosp. Electron. Syst. Mag.*, vol. 28, no. 6, pp. 38–41, Jun. 2013.
[8] K. Pesyna, Z. Kassas, and T. Humphreys, "Constructing a continuous phase time history from TDMA signals for opportunistic navigation," in *Proc. IEEE/ION PLANS*, Apr. 2012, pp. 1209–1220.
[9] P. Thevenon, S. Damien, O. Julien, C. Macabiau, M. Bousquet, L. Ries, and S. Corazza, "Positioning using mobile TV based on the DVB-SH standard," *NAVIGATION, J. Inst. Navig.*, vol. 58, no. 2, pp. 71–90, 2011.
[10] C. Yang, T. Nguyen, E. Blasch, and D. Qiu, "Assessing terrestrial wireless communications and broadcast signals as signals of opportunity for positioning and navigation," in *Proc. ION GNSS*, Sep. 2012, pp. 3814–3824.
[11] H. Durrant-Whyte and T. Bailey, "Simultaneous localization and mapping: Part I," *IEEE Robot. Autom. Mag.*, vol. 13, no. 2, pp. 99–110, Jun. 2006.
[12] T. Bailey and H. Durrant-Whyte, "Simultaneous localization and mapping: Part II," *IEEE Robot. Autom. Mag.*, vol. 13, no. 3, pp. 108–117, Sep. 2006.
[13] P. Corcoran, A. Winstanley, P. Mooney, and R. Middleton, "Background foreground segmentation for SLAM," *IEEE Trans. Intell. Transp. Syst.*, vol. 12, no. 4, pp. 1177–1183, Dec. 2011.
[14] A. Vu, A. Ramanandan, A. Chen, J. Farrell, and M. Barth, "Real-time computer vision/DGPS-aided inertial navigation system for lane-level vehicle navigation," *IEEE Trans. Intell. Transp. Syst.*, vol. 13, no. 2, pp. 899–913, Jun. 2012.
[15] J. J. Spilker, Jr., *Global Positioning System: Theory and Applications*. Washington, DC, USA: Amer. Inst. Aeronaut. Astronaut., 1996, ch. 2, pp. 57–119.
[16] J. Andrade-Cetto and A. Sanfeliu, "The effects of partial observability in SLAM," in *Proc. IEEE Int. Conf. Robot. Autom.*, Apr. 2004, vol. 1, pp. 397–402.
[17] J. Andrade-Cetto and A. Sanfeliu, "The effects of partial observability when building fully correlated maps," *IEEE Trans. Robot.*, vol. 21, no. 4, pp. 771–777, Aug. 2005.
[18] T. Vida-Calleja, M. Bryson, S. Sukkarieh, A. Sanfeliu, and J. Andrade-Cetto, "On the observability of bearing-only SLAM," in *Proc. IEEE Int. Conf. Robot. Autom.*, Apr. 2007, vol. 1, pp. 4114–4119.
[19] K. Lee, W. Wijesoma, and I. Javier, "On the observability and observability analysis of SLAM," in *Proc. IEEE Int. Conf. Intell. Robots Syst.*, Oct. 2006, vol. 1, pp. 3569–3574.
[20] Z. Wang and G. Dissanayake, "Observability analysis of SLAM using Fisher information matrix," in *Proc. IEEE Int. Conf. Control, Autom., Robot. Vis.*, Dec. 2008, vol. 1, pp. 1242–1247.
[21] L. Perera, A. Melkumyan, and E. Nettleton, "On the linear and nonlinear observability analysis of the SLAM problem," in *Proc. IEEE Int. Conf. Mechatron.*, Apr. 2009, vol. 1, pp. 1–6.
[22] L. Perera and E. Nettleton, "On the nonlinear observability and the information form of the SLAM problem," in *Proc. IEEE Int. Conf. Intell. Robots Syst.*, Oct. 2009, vol. 1, pp. 2061–2068.
[23] L. Perera and E. Nettleton, "On stochastically observable directions of the estimation theoretic SLAM state space," in *Proc. IEEE/RSJ Int. Conf. Intell. Robots Syst.*, Oct. 2010, pp. 4324–4331.
[24] G. Huang, A. Mourikis, and S. Roumeliotis, "Observability-based rules for designing consistent EKF SLAM estimators," *Int. J. Robot. Res.*, vol. 29, no. 5, pp. 502–528, Apr. 2010.
[25] D. Goshen-Meskin and I. Bar-Itzhack, "Observability analysis of piecewise constant systems—Part I: Theory," *IEEE Trans. Aerosp. Electron. Syst.*, vol. 28, no. 4, pp. 1056–1067, Oct. 1992.
[26] Z. Kassas and T. Humphreys, "Observability analysis of opportunistic navigation with pseudorange measurements," in *Proc. AIAA Guid., Navig. Control Conf.*, Aug. 2012, vol. 1, pp. 1209–1220.
[27] Z. Kassas and T. Humphreys, "Observability and estimability of collaborative opportunistic navigation with pseudorange measurements," in *Proc. ION GNSS*, Sep. 2012, pp. 621–630.
[28] R. Hermann and A. Krener, "Nonlinear controllability and observability," *IEEE Trans. Autom. Control*, vol. AC-22, no. 5, pp. 728–740, Oct. 1977.
[29] M. Anguelova, "Observability and identifiability of nonlinear systems with applications in biology," Ph.D. dissertation, Chalmers Univ. Technol., Göteborg Univ., Gothenburg, Sweden, 2007.
[30] W. Rugh, *Linear System Theory*, 2nd ed. Upper Saddle River, NJ, USA: Prentice-Hall, 1996.
[31] Y. Bar-Shalom, X. Li, and T. Kirubarajan, *Estimation With Applications to Tracking and Navigation*. New York, NY, USA: Wiley, 2002.
[32] F. Ham and R. Brown, "Observability, eigenvalues, and Kalman filtering," *IEEE Trans. Aerosp. Electron. Syst.*, vol. AES-19, no. 2, pp. 269–273, Mar. 1983.
[33] J. Barnes, A. Chi, R. Andrew, L. Cutler, D. Healey, D. Leeson, T. McGunigal, J. Mullen, W. Smith, R. Sydnor, R. Vessot, and G. Winkler, "Characterization of frequency stability," *IEEE Trans. Instrum. Meas.*, vol. IM-20, no. 2, pp. 105–120, May 1971.
[34] A. Thompson, J. Moran, and G. Swenson, *Interferometry and Synthesis in Radio Astronomy*, 2nd ed. Hoboken, NJ, USA: Wiley, 2001.
[35] R. Brown and P. Hwang, *Introduction to Random Signals and Applied Kalman Filtering*, 3rd ed. Hoboken, NJ, USA: Wiley, 2002.
[36] M. Psiaki and S. Mohiuddin, "Modeling, analysis, and simulation of GPS carrier phase for spacecraft relative navigation," *J. Guid., Control, Dyn.*, vol. 30, no. 6, pp. 1628–1639, Nov./Dec. 2007.
[37] Z. Kassas, "Discretisation of continuous-time dynamic multi-input multi-output systems with non-uniform delays," *IET Control Theory Appl.*, vol. 5, no. 14, pp. 1637–1647, Sep. 2011.
[38] J. Caffery and G. Stuber, "Overview of radiolocation in CDMA cellular systems," *IEEE Commun. Mag.*, vol. 36, no. 4, pp. 38–45, Apr. 1998.

[39] E. Costa, "Simulation of the effects of different urban environments on GPS performance using digital elevation models and building databases," *IEEE Trans. Intell. Transp. Syst.*, vol. 12, no. 3, pp. 819–829, Sep. 2011.
[40] G. Seco-Granados, J. Lopez-Salcedo, D. Jimenez-Banos, and G. Lopez-Risueno, "Challenges in indoor global navigation satellite systems: Unveiling its core features in signal processing," *IEEE Signal Process. Mag.*, vol. 29, no. 2, pp. 108–131, Mar. 2012.
[41] G. De Angelis, G. Baruffa, and S. Cacopardi, "GNSS/cellular hybrid positioning system for mobile users in urban scenarios," *IEEE Trans. Intell. Transp. Syst.*, vol. 14, no. 1, pp. 313–321, Mar. 2013.
[42] T. E. Humphreys, J. Bhatti, T. Pany, B. Ledvina, and B. O'Hanlon, "Exploiting multicore technology in software-defined GNSS receivers," in *Proc. ION GNSS*, Sep. 2009, pp. 326–338.

Zaher (Zak) M. Kassas (S'98–M'08–SM'11) received the B.E. (Hons.) degree in electrical engineering from Lebanese American University, New York, NY, USA; the M.S. degree in electrical and computer engineering from The Ohio State University, Columbus, OH, USA; and the M.S.E. degree in aerospace engineering from The University of Texas at Austin, Austin, TX, USA. He is currently working toward the Ph.D. degree with the Department of Electrical and Computer Engineering, The University of Texas at Austin.

From 2004 to 2010, he was a Research and Development Engineer with the Control Design and Dynamical Systems Simulation Group, National Instruments Corporation. From 2008 to 2011, he was an adjunct Professor with Texas State University, San Marcos, TX. His research interests include estimation, navigation, autonomous vehicles, control systems, and intelligent transporation systems.

Todd E. Humphreys (M'12) received the B.S. and M.S. degrees in electrical and computer engineering from Utah State University, Logan, UT, USA, and the Ph.D. degree in aerospace engineering from Cornell University, Ithaca, NY, USA.

He is currently an Assistant Professor with the Department of Aerospace Engineering and Engineering Mechanics, The University of Texas at Austin, Austin, TX, USA, and the Director of the University of Texas Radionavigation Laboratory, The University of Texas at Austin. His research interests include estimation and filtering, Global Navigation Satellite System (GNSS) technology, GNSS-based study of the ionosphere and the neutral atmosphere, and GNSS security and integrity.